Predefined time tracking control of underactuated surface vessel with input saturation

HUANG Xiuying[1], *LIU Haitao*[*1,2], *TIAN Xuehong*[1,2]

1 School of Mechanical Engineering, Guangdong Ocean University, Zhanjiang 524088, China
2 Shenzhen Institute of Guangdong Ocean University, Shenzhen 518120, China

Abstract: [**Objectives**] To solve the trajectory tracking problem of underactuated surface vessels (USVs) under the condition of model uncertainty, strong coupling characteristics and controller input saturation, this study proposes a predefined time tracking control method for USVs based on input saturation. [**Methods**] Due to the non-zero diagonal terms and strong coupling characteristics of the USV model, coordinate transformation is introduced to transform the system model into a diagonal form. To obtain the predetermined tracking performance, the predefined time performance function is combined with the barrier Lyapunov function (BLF) to ensure transient and stable tracking performance. Self-structuring neural networks (SSNN) are used to approximate unknown external disturbances and complex continuous unknown nonlinear terms, and deal with the impact of actuator saturation, thus ensuring the tracking performance of the control system. Moreover, the number of SSNN neurons can be adjusted online, reducing the computational burden on the control system. [**Results**] Based on the Lyapunov stability theory, it is proven that the closed-loop system is bounded stable in a predefined time, and the tracking error is always within the constraint range. [**Conclusions**] The simulation results show that the proposed control strategy is effective and has good tracking performance.

Key words: underactuated surface vessel; predefined-time performance function; barrier Lyapunov function; self-structuring neural network; input saturation; predefined-time control

CLC number：U664.82

0　Introduction

In the context of large-scale development of marine resources, underactuated surface vessels (USVs) have widely been used for maritime rescue, maritime reconnaissance, target search and tracking, and marine environmental investigation[1]. Trajectory tracking control of USVs has attracted much attention for many years. Dynamics models of USVs are highly nonlinear and strongly coupled. Complexity and changeability of marine environment and uncertainty of ship modeling increase the difficulty of controller design. In addition, underactuation of USVs places higher requirements on controller design [2].

In the face of complex marine environment, whether USVs are equipped with fast and accurate tracking performance greatly affects their accuracy in carrying out maritime tasks. Based on the assumption of accurate dynamics model of ships, Wang et al. [3] realized the asymptotic convergence of USV tracking errors. In fact, due to complex hydrodynamic moments and wind effects, ship models are highly nonlinear. Thus, it is difficult to obtain accurate model information. Considering uncertainty of ship modeling and disturbances from external environment, References [4-8] maintained uniform ultimate boundedness of tracking errors. Although convergence rates of tracking errors and size of residual sets can be adjusted, it is impossible to determine accuracy and convergence rates of tracking errors in advance. References [9-11] controlled tracking errors to fall into a pre-selected range at a specified rate, further improving the

transient- and steady-state tracking accuracy of ships. However, due to slow convergence of an exponential performance function, it is impossible to guarantee that tracking errors can converge to desired accuracy within a preset time. In fact, high tracking accuracy needs to be achieved within a predefined time. By introducing a barrier Lyapunov function (BLF), References [12-13] ensured that tracking errors of USVs satisfied preset accuracy; however, system errors were asymptotically convergent. By introducing tan-type and log-type barrier Lyapunov functions (TBLF), References [14-16] solved error constraints, and proposed a finite-time stability control strategy. However, finite-time stability is affected by initial states. Zhang et al. [17] further considered fixed-time stability of under-actuated ship control systems based on a log-type BLF. However, fixed-time stability is too conservative. Moreover, what cannot be ignored is that log-type BLFs is restricted functionally while tan-type one complicates controller design [18]. In actual applications, motion of USVs is often restrained by output saturation of actuators. Thus, in the case of actuator output saturation, how to realize fast and accurate tracking of USVs is a problem worth studying. References [19-20] further considered output saturation of actuators while ensuring transient- and steady-state tracking accuracy of USVs.

It is difficult to obtain accurate USV model information by hydrodynamics. In view of this problem, to approximate nonlinear damping terms, Zhang et al. [21] reconstructed uncertainty terms of dynamic models of ships by using a radial-basis-function neural network, realizing finite-time tracking control of underactuated ships. To estimate external environmental disturbances, References [22-24] designed a disturbance observer. In References [25-26], an adaptive neural network was used to approximate unknown nonlinear damping terms and external environmental disturbances. However, in neural-network-based compensation strategies, many parameters for estimation and identification are updated online, which greatly increases computational costs of control systems. In Reference [27], a self-structuring fuzzy neural network was introduced to compensate for unknown dynamics of ships. This method effectively reduces calculation burden of control systems by generating or pruning fuzzy rules online through structural learning criteria. However, self-structuring fuzzy

neural networks require the construction of complex fuzzy rules. Radial-basis-function neural networks (RBFNNs) are characterized by approximation of uncertain dynamics. With a fixed network structure, a conventional RBFNN can hardly deal with complex unknown time-varying dynamics effectively, and excessive neurons increase computational burden of control systems. Therefore, the combination of self-structuring criteria and RBF is worthy of further discussion.

Based on the above discussion, in view of trajectory tracking control of USVs, this paper proposed a predefined-time trajectory tracking control method based on a self-structuring neural network under the influence of model uncertainties and unknown time-varying disturbances. Different from an exponential decay performance function, a performance function with arbitrarily predefined time convergence was introduced to provide a predefined constraint specification for error tracking. In addition, a BLF was used as the boundary function of predefined constraints to meet defined tracking accuracy. Dynamic surface control was employed in the control design to avoid "computational explosion" caused by the derivation of virtual control laws [28]. On this basis, an adaptive predefined time filter was proposed. Moreover, in view of input saturation of USVs, a self-structuring neural network (SSNN) was adopted to approximate uncertainties of ship models, time-varying disturbances of external environment, and influence of input saturation. Number of neurons can be adjusted online to optimize the structure of the neural network to reduce computational burden of the system. In view of trajectory tracking control of USVs, this paper proposed a predefined-time stabilization method to ensure stability and uniform boundedness of the closed-loop control system within a predefined time. Predefined-time stability was analyzed by constructing a Lyapunov function. Simulation tests were carried out based on a desired trajectory to verify effectiveness and tracking effect of the control method.

1　Preliminary knowledge and problem description

1.1　Preliminary knowledge

Lemma 1: Consider a nonlinear system $\dot{x}_0 = f(t, x_0, d)$, where x_0 is a system state and d is an uncertain term. Define a continuous positive definite function

$V(\boldsymbol{x}_0)$ and design parameters $0 < \gamma < 1$, $T_c > 0$ and $0 < \vartheta < \infty$, which satisfy the following condition [29]:

$$\dot{V} \leqslant -\frac{\pi}{\gamma T_c}\left(V^{1-\gamma/2} + V^{1+\gamma/2}\right) + \vartheta \tag{1}$$

Then, the trajectory of $\dot{\boldsymbol{x}}_0 = f(t, \boldsymbol{x}_0, \boldsymbol{d})$ is actually predefined-time stable, and the convergence region is given by Eq. (2).

$$\left\{\lim_{t \to T_c'} \boldsymbol{x}_0 | V \leqslant \min\left\{\left(\frac{2\gamma T_c \vartheta}{\pi}\right)^{\frac{2}{2-\gamma}}, \left(\frac{2\gamma T_c \vartheta}{\pi}\right)^{\frac{2}{2+\gamma}}\right\}\right\} \tag{2}$$

where T_c' is the establishment time, satisfying $T_c' < T_{\max} = \sqrt{2}T_c$, and $T_{\max}$ is the upper limit.

Lemma 2: For any defined $k > 0$, $h \geqslant 0$, and $y > 0$, the following inequality [30] is satisfied:

$$h^k(y - h) \leqslant \frac{1}{1+k}\left(y^{1+k} - h^{1+k}\right) \tag{3}$$

For $k > 1$, $h > 0$, and $y \leqslant h$, the following condition is satisfied:

$$(h - y)^k \leqslant y^k - h^k \tag{4}$$

Lemma 3: For any $\mathfrak{I} \in \mathbf{R}$, there is the following inequality [31]:

$$\begin{cases} \sum_{i=1}^{m} |\mathfrak{I}_i|^{1+p} \geqslant \left(\sum_{i=1}^{m} |\mathfrak{I}|\right)^{2^{(1+p)/2}}, & 0 < p \leqslant 1 \\ \sum_{i=1}^{m} |\mathfrak{I}_i|^p \geqslant m^{1-p}\left(\sum_{i=1}^{m} |\mathfrak{I}|\right)^p, & p > 1 \end{cases} \tag{5}$$

Lemma 4: For any $\ell \in \mathbf{R}^+$ and $X \in \mathbf{R}$, the following inequality holds [32]:

$$0 < |X| - X\tanh\left(\frac{X}{\ell}\right) \leqslant \kappa\ell \tag{6}$$

where $\kappa = 0.278\,5$, satisfying $\kappa = \mathrm{e}^{-(\kappa+1)}$.

1.2 SSNN

According to relevant research [33-34], in RBFNNs, more neurons will lead to better approximation to unknown nonlinear functions. Noteworthily, not all neurons are effective. Ineffective neurons not only fail to improve approximation performance but also increase computational costs of control systems. Different from RBFNNs, SSNNs can adjust number of neurons online. By judging effectiveness of neurons, SSNNs increase or delete neurons independently, thus effectively reducing computational burden of systems. Moreover, they can achieve good approximation performance. The approximation function of an SSNN is given by:

$$f(\boldsymbol{x}) = \boldsymbol{W}^{\mathrm{T}}\boldsymbol{S}(\boldsymbol{x}) + \varepsilon(\boldsymbol{x}) \tag{7}$$

$$\boldsymbol{W} = \arg\ \min\left\{\sup_{x \in \mathbf{R}}\left|f(\boldsymbol{x}) - \hat{\boldsymbol{W}}^{\mathrm{T}}\boldsymbol{S}(\boldsymbol{x})\right|\right\} \tag{8}$$

where x represents the input of the SSNN; $\varepsilon(x)$ is an approximation error; $\boldsymbol{W} \in \mathbf{R}$ is an ideal weight; number of SSNN neurons is $N > 1$; $\hat{\boldsymbol{W}}$ is the estimation of $\boldsymbol{W}$; $\boldsymbol{S}(\boldsymbol{x}) = [S_1(\boldsymbol{x}), S_2(\boldsymbol{x}), ..., S_N(\boldsymbol{x})]^{\mathrm{T}}$ is a basis function vector; $S_i(\boldsymbol{x})$ is a Gaussian function, expressed as

$$S_i(\boldsymbol{x}) = \exp\left(-\frac{\|\boldsymbol{x} - \boldsymbol{c}_i\|^2}{b_i^2}\right), \ i = 1, 2, \ldots, N \tag{9}$$

where b_i is breadth of the Gaussian basis function; c_i is the central vector of the Gaussian basis function.

Hypothesis 1: The ideal weight of the SSNN is bounded, with $\|\boldsymbol{W}\| \leqslant W^*$, where W^* is a positive constant. $\varepsilon(x)$ is an approximation error, satisfying $\varepsilon(x) \leqslant \varepsilon^*$, where ε^* is a positive constant.

Define a neuron with the best activation effect as $S_{\mathrm{M}} = \max\limits_{1 \leqslant k \leqslant N} S_k$, the split threshold of the SSNN as $\varUpsilon_s \in (0, 1)$, and the decay threshold of the SSNN as $\varUpsilon_d \in (0, 1)$, with $\varUpsilon_s > \varUpsilon_d$. The neuron-splitting strategy first judges whether the neuron with the best activation effect exceeds the preset threshold. If it is less than the split threshold (i.e., $S_{\mathrm{M}} < \varUpsilon_s$), the neuron fails to reach the ideal activation effect, and then the neuron-splitting strategy is carried out to obtain a better approximation effect. The newly split neuron is represented by S_{new}, and parameters of the new neuron are as follows:

$$\begin{cases} \boldsymbol{c}_{\mathrm{new}} = \dfrac{\boldsymbol{x}_{\mathrm{M}} + \boldsymbol{c}_{\mathrm{M}}}{2} \\ b_{\mathrm{new}} = b_{\mathrm{M}} \\ W_{\mathrm{new}} = 0 \end{cases} \tag{10}$$

where c_{new} is a central vector of the Gaussian basis function of the new neuron; b_{new} is breadth of the Gaussian basis function of the new neuron; $\boldsymbol{x}_{\mathrm{M}}$, $\boldsymbol{c}_{\mathrm{M}}$ and b_{M} are parameters of the best activation; W_{new} is the initial value of the weight of the new neuron.

The neuron decay parameter is defined as I_{n}, with an initial value of 1. The decay threshold $\varUpsilon_d$ functions to determine whether to implement the neuron-decaying strategy or not. I_{n} observes the following rule:

$$I_{\mathrm{n}} = \begin{cases} \varLambda I_{\mathrm{n}}, & S_i \leqslant p_{\mathrm{d}} \\ 1, & S_i > p_{\mathrm{d}} \end{cases}, \ i = 1, 2, \ldots, N \tag{11}$$

where $\varLambda$ is a decay coefficient; p_{d} is a self-defining value; if $I_{\mathrm{n}} \leqslant \varUpsilon_d$ the neuron-decaying strategy will be triggered to delete the n-th neuron.

Fig. 1 illustrates the flowchart of the SSNN algorithm. The function $\hat{\boldsymbol{F}}$ is the approximation of the unknown function $f(\boldsymbol{x}) = \boldsymbol{W}^{\mathrm{T}}\boldsymbol{S}(\boldsymbol{x}) + \varepsilon(\boldsymbol{x})$. In the case of a more complex unknown nonlinear function, it is necessary to add more effective

neurons and delete ineffective ones. By increasing $\varUpsilon_s$ and decreasing $\varUpsilon_d$, we can add effective neurons to achieve a better approximation effect, without bringing excessive computational cost to the control system. In addition, we can decrease $\varUpsilon_s$ and increase $\varUpsilon_d$ to delete more ineffective neurons without affecting the approximation effect, so as to reduce computational cost of the control system.
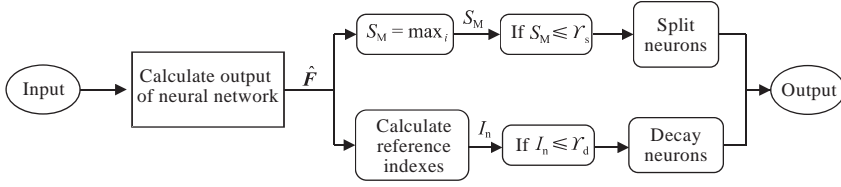

Fig. 1   SSNN algorithm flowchart

1.3   Mathematical model of USV

According to the mathematical model of a USV, strong coupling caused by non-diagonal terms in the mass inertial matrix is solved by coordinate transformation. Kinematics and dynamics models of the USV are as follows [35]:

$$\begin{cases} \dot{\boldsymbol{\eta}} = \boldsymbol{J}(\psi)\boldsymbol{v} \\ \boldsymbol{M}\dot{\boldsymbol{v}} = -\boldsymbol{C}(\boldsymbol{v})\boldsymbol{v} - \boldsymbol{D}(\boldsymbol{v})\boldsymbol{v} + \boldsymbol{\tau}_d + \boldsymbol{\tau}_c \end{cases} \qquad (12)$$

$$\boldsymbol{J}(\psi) = \begin{bmatrix} \cos(\psi) & -\sin(\psi) & 0 \\ \sin(\psi) & \cos(\psi) & 0 \\ 0 & 0 & 1 \end{bmatrix}$$

where

$$\boldsymbol{M} = \begin{bmatrix} m_{11} & 0 & 0 \\ 0 & m_{22} & m_{23} \\ 0 & m_{32} & m_{33} \end{bmatrix}$$

$$\boldsymbol{C}(\boldsymbol{v}) = \begin{bmatrix} 0 & 0 & C_{13} \\ 0 & 0 & C_{23} \\ C_{31} & C_{32} & 0 \end{bmatrix}$$

$$\boldsymbol{D}(\boldsymbol{v}) = \begin{bmatrix} d_{11} & 0 & 0 \\ 0 & d_{22} & d_{23} \\ 0 & d_{32} & d_{33} \end{bmatrix}$$

where $\boldsymbol{\eta} = [x,y,\psi]^{\mathrm{T}}$ refers to the position and yaw angle of the USV; specifically, (x,y) are the position coordinates and ψ is the yaw angle; $\boldsymbol{J}(\psi)$ is a rotation matrix between geodetic and hull-fixed coordinate systems; $\boldsymbol{v} = [u,v,r]^{\mathrm{T}}$ is a velocity vector, with u, v and r being forward velocity, lateral velocity, and yaw angular velocity, respectively; $\boldsymbol{M}$ is a mass inertial matrix; $\boldsymbol{C}(\boldsymbol{v})$ is a centripetal matrix of Coriolis force. $\boldsymbol{D}(\boldsymbol{v})$ is a matrix of hydrodynamic damping coefficients . $m_{11} = m_0 - X_{\dot{u}}$, $m_{22} = m_0 - Y_{\dot{v}}$, $m_{23} = m_0 x_g - Y_{\dot{r}}$, $m_{33} = I_z - N_{\dot{r}}$, $d_{11} = -X_u - X_{|u|u}|u| - X_{uuu}u^2$, $d_{22} = -Y_v - Y_{|v|v}|v| - Y_{|r|v}|r|$, $d_{23} = -Y_r - Y_{|v|r}|v| - Y_{|r|r}|r|$, $d_{32} = -N_v - N_{|v|v}|v| - N_{|r|v}|r|$, $d_{33} = -N_r - N_{|v|v}|v| - N_{|r|r}|r|$, , where m_0 is mass of the USV. $X_{\dot{u}}$, $Y_{\dot{v}}$, $Y_{\dot{r}}$, and N_r are additional mass; x_g is the deviation between the center of gravity of the USV and the origin of the hull-fixed coordinate system; I_z is the moment of inertia in the yaw direction; $X(\cdot)$, $Y(\cdot)$ and $N(\cdot)$ are linear and quadratic hydrodynamic damping coefficients of forward, lateral, and yawing movements; $\boldsymbol{\tau}_d = [\tau_{du}, \tau_{dv}, \tau_{dr}]^{\mathrm{T}}$ is a vector of external time-varying disturbances; $\boldsymbol{\tau}_c = [\tau_{cu}, 0, \tau_{cr}]^{\mathrm{T}}$ is a control input under input saturation. Actuator output saturation is defined as follows:

$$\tau_{c\iota} = \begin{cases} \tau_\iota^+, & \tau_\iota > \tau_\iota^+ \\ \tau_\iota, & \tau_\iota^- \leqslant \tau_\iota \leqslant \tau_\iota^+ \\ \tau_\iota^-, & \tau_\iota < \tau_\iota^+ \end{cases} \qquad (13)$$

where $\tau_\iota(\iota = u, r)$ is a control instruction in the case of no input saturation; τ_ι^+ and τ_ι^- are upper and lower bounds of input saturation, respectively.

Since the saturation model Eq. (13) cannot be directly used for backstepping design, a smooth model is defined to describe the asymmetrically saturated nonlinear model [36].

$$\tau_{c\iota} = \tau_{\mathrm{Mc}\iota} \times \mathrm{erf}\left(\frac{\sqrt{\pi}}{2\tau_{\mathrm{Mc}\iota}}\tau_\iota\right) \qquad (14)$$

where

$$\tau_{\mathrm{Mc}\iota} = (\tau_\iota^+ + \tau_\iota^-)/2 + ((\tau_\iota^+ - \tau_\iota^-)/2)\,\mathrm{sign}(\tau_\iota), \ \iota = u, r$$

$$\mathrm{erf}(\hat{x}) = \frac{2}{\sqrt{\pi}}\int_0^{\hat{x}} \mathrm{e}^{-t^2}\mathrm{d}t$$

where $\mathrm{sign}(\cdot)$ is a standard symbolic function; $\mathrm{erf}(\cdot)$ is a Gaussian error function. Symmetric and asymmetric saturation models can be obtained by adjusting τ_ι^+ and τ_ι^-. In the case of $|\tau_\iota^+| = |\tau_\iota^-|$, a symmetric saturation model can be obtained. In the case of $|\tau_\iota^+| \neq |\tau_\iota^-|$, an asymmetric saturation model can be obtained. Fig. 2 shows that the saturation model Eq. (13) is of smooth saturation limits, where $\tau_\iota^+=8$, $\tau_\iota^-=-4$, and the input signal is $\tau_{\mathrm{Mc}}=25\sin(1.5t)$ N.

With the further consideration about the error $\varDelta = \boldsymbol{\tau} - \boldsymbol{\tau}_c$ of input saturation, where $\boldsymbol{\tau}$ is a control input in the case of no input saturation, the dynamics model can be rewritten as

$$\boldsymbol{M}\dot{\boldsymbol{v}} = -\boldsymbol{C}(\boldsymbol{v})\boldsymbol{v} - \boldsymbol{D}(\boldsymbol{v})\boldsymbol{v} + \boldsymbol{\tau}_d + \boldsymbol{\tau} - \varDelta \qquad (15)$$

where $\boldsymbol{\tau} = [\tau_u, 0, \tau_r]^{\mathrm{T}}$; $\varDelta = [\varDelta_u, 0, \varDelta_r]^{\mathrm{T}}$.

Under the influence of the mass inertial matrix

Fig. 2   Saturation functions

Fig. 3   Schematic diagram of USV trajectory tracking
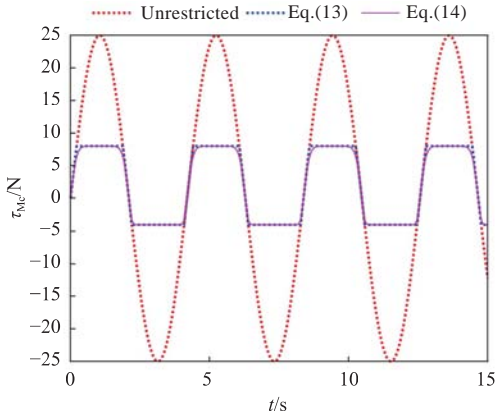
M, lateral and yawing velocity will affect control input jointly, which increases the difficulty of controller design. For this reason, coordinate transformation is introduced to solve USV coupling. Coordinate transformation of a USV is described as follows [34]:

$$\begin{cases} \bar{x} = x + \chi\cos(\psi) \\ \bar{y} = y + \chi\sin(\psi) \\ \bar{\upsilon} = \upsilon + \chi r \end{cases} \quad (16)$$

where $\chi = m_{23}/m_{22}$.

With Eq. (16), the mathematical model of USV can be transformed into

$$\begin{cases} \dot{\bar{\eta}} = J(\psi)\bar{\upsilon} \\ \dot{\bar{\upsilon}} = f + d + \tau' - \varDelta' \end{cases} \quad (17)$$

where

$$\bar{\eta} = [\bar{x}, \bar{y}, \psi]^{\mathrm{T}}, \quad \bar{\upsilon} = [u, \bar{\upsilon}, r]^{\mathrm{T}}, \quad f = [f_1, f_2, f_3]^{\mathrm{T}}$$

$$\tau' = [\zeta_u\tau_u, 0, \zeta_r\tau_r]^{\mathrm{T}}, \quad \varDelta' = [\zeta_u\varDelta_u, 0, \zeta_r\varDelta_r]^{\mathrm{T}}, \quad d = [d_u, d_v, d_r]^{\mathrm{T}}$$

$$d_u = \xi_u\tau_{du}, \quad d_v = \xi_v\tau_{dv}, \quad d_r = \xi_r(\tau_{dr} - \chi\tau_{dv})$$

$$\begin{cases} f_1 = (m_{22}(\bar{\upsilon} - \chi r)r + m_{23}r^2 - d_{11}u)/m_{11} \\ f_2 = (-m_{11}ur - d_{22}(\bar{\upsilon} - \chi r) - d_{23}r)/m_{22} \\ f_3 = ((m_{11}m_{22} - m_{22}^2)u(\bar{\upsilon} - \chi r) + (m_{11}m_{32} - \quad (18) \\ \qquad m_{23}m_{22})ur - (d_{33}r + d_{32}(\bar{\upsilon} - \chi r))m_{22} + \\ \qquad (d_{23}r + d_{22}(\bar{\upsilon} - \chi r))m_{23})/V \end{cases}$$

where $f = [f_1, f_2, f_3]^{\mathrm{T}}$ is the uncertainty term of the USV model. $V = m_{22}m_{33} - m_{23}m_{32}$.

Hypothesis 2: The external disturbance $d = [d_u, d_v, d_r]^{\mathrm{T}}$ is bounded, $d_i \leqslant d_{i\max}$, $i = u, v, r$.

Hypothesis 3: The desired position $\eta_{\mathrm{d}} = [x_{\mathrm{d}}, y_{\mathrm{d}}, \psi_{\mathrm{d}}]^{\mathrm{T}}$ and $\dot{\eta}_{\mathrm{d}}$ are bounded.

In Fig. 3, (x, y) refers to the actual position of the USV; $(x_{\mathrm{d}}, y_{\mathrm{d}})$ refers to the desired position; ψ is the actual heading angle of the USV; ψ_{d} is the desired heading angle; ψ_{e} is the heading-angle error.

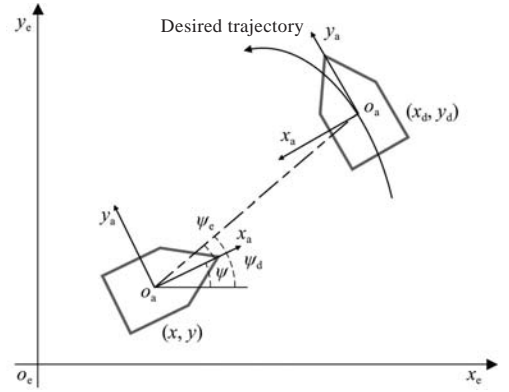The tracking error after coordinate transformation is defined as follows:

$$\begin{cases} \bar{x}_{\mathrm{e}} = x_{\mathrm{d}} - \bar{x}, \quad \bar{y}_{\mathrm{e}} = y_{\mathrm{d}} - \bar{y} \\ \psi_{\mathrm{e}} = \psi_{\mathrm{d}} - \psi, \quad \bar{E} = \sqrt{\bar{x}_{\mathrm{e}}^2 + \bar{y}_{\mathrm{e}}^2} \end{cases} \quad (19)$$

where $(\bar{x}_{\mathrm{e}}, \bar{y}_{\mathrm{e}})$ is the position tracking error after coordinate transformation; $\bar{E}$ is the line-of-sight (LOS) guidance range. The desired heading angle ψ_{d} is defined as follows [18]:

$$\begin{cases} \psi_{\mathrm{e}} = \arctan2(\tilde{y}_{\mathrm{e}}, \tilde{x}_{\mathrm{e}}) \\ \psi_{\mathrm{d}} = \psi + \psi_{\mathrm{e}} \end{cases} \quad (20)$$

where

$$\begin{bmatrix} \tilde{x}_{\mathrm{e}} \\ \tilde{y}_{\mathrm{e}} \end{bmatrix} = \begin{bmatrix} \cos\psi & \sin\psi \\ -\sin\psi & \cos\psi \end{bmatrix} \begin{bmatrix} \bar{x}_{\mathrm{e}} \\ \bar{y}_{\mathrm{e}} \end{bmatrix} \quad (21)$$

$$\mathrm{atan2}(\tilde{y}_{\mathrm{e}}, \tilde{x}_{\mathrm{e}}) = \begin{cases} \arctan\left(\dfrac{\tilde{y}_{\mathrm{e}}}{\tilde{x}_{\mathrm{e}}}\right), & \tilde{x}_{\mathrm{e}} > 0 \\ \arctan\left(\dfrac{\tilde{y}_{\mathrm{e}}}{\tilde{x}_{\mathrm{e}}}\right) + \pi, & \tilde{x}_{\mathrm{e}} < 0, \tilde{y}_{\mathrm{e}} \geqslant 0 \\ \arctan\left(\dfrac{\tilde{y}_{\mathrm{e}}}{\tilde{x}_{\mathrm{e}}}\right) - \pi, & \tilde{x}_{\mathrm{e}} < 0, \tilde{y}_{\mathrm{e}} < 0 \quad (22) \\ +\dfrac{\pi}{2}, & \tilde{x}_{\mathrm{e}} = 0, \tilde{y}_{\mathrm{e}} > 0 \\ -\dfrac{\pi}{2}, & \tilde{x}_{\mathrm{e}} = 0, \tilde{y}_{\mathrm{e}} < 0 \\ \text{undefined}, & \tilde{x}_{\mathrm{e}} = 0, \tilde{y}_{\mathrm{e}} = 0 \end{cases}$$

2   Controller design

2.1   Predefined-time state constraint controller

Most of the performance constraints are solved by exponential decay performance functions to ensure that tracking errors are limited to a preset range. However, such functions can only guarantee that tracking errors converge to a preset range in infinite time, with no guarantee to achieve preset tracking performance in predefined time. For better tracking performance, a predefined-time performance function is introduced to ensure that tracking errors can reach desired tracking accuracy within a predefined time. The predefined-time performance function is defined as follows [37]:

$$\sigma_i = \begin{cases} \sigma_{i0}e^{1-\frac{T_h}{T_h-t}} + \sigma_{i\infty}, & t \geqslant T_h \\ \sigma_{i\infty}, & t \geqslant T_h \end{cases} \quad (23)$$

where $\sigma_{i0} > \sigma_{i\infty} > 0 (i = u,r)$; T_h is freely set time. Therefore, tracking errors satisfy the following conditions:

$$\begin{cases} \bar{E} < \sigma_u \\ -\sigma_r < \psi_e < \sigma_r \end{cases} \quad (24)$$

To obtain better tracking performance, we constructed the following time-varying BLF [38]:

$$V_u = \frac{\sigma_u^2 \bar{E}}{\sigma_u^2 - \bar{E}^2}, \quad V_r = \frac{\sigma_r^2 \psi_e}{\sigma_r^2 - \psi_e^2} \quad (25)$$

The following Lyapunov function is considered:

$$V_1 = \frac{1}{2}V_u^2 + \frac{1}{2}V_r^2 \quad (26)$$

Then the first derivative of V_1 is given by

$$\dot{V}_1 = V_u\dot{V}_u + V_r\dot{V}_r =$$
$$\frac{\sigma_u^2\bar{E}}{\sigma_u^2 - \bar{E}^2}\frac{(\sigma_u^4 + \sigma_u^2\bar{E}^2)\dot{\bar{E}} - 2\sigma_u\dot{\sigma}_u\bar{E}^3}{(\sigma_u^2 - \bar{E}^2)^2} +$$
$$\frac{\sigma_r^2\psi_e}{\sigma_r^2 - \psi_e^2}\frac{(\sigma_r^4 + \sigma_r^2\psi_e^2)\dot{\psi}_e - 2\sigma_r\dot{\sigma}_r\psi_e^3}{(\bar{\sigma}_r^2 - \psi_e^2)^2} =$$
$$\frac{\sigma_u^2\bar{E}}{\sigma_u^2 - \bar{E}^2}((\sigma_u^4 + \sigma_u^2\bar{E}^2)(\dot{x}_d\cos(\psi_d)+$$
$$\dot{y}_d\sin(\psi_d) - u\cos(\psi_e) - \bar{v}\sin(\psi_e)) -$$
$$2\sigma_u\dot{\sigma}_u\bar{E}^3)/(\sigma_u^2 - \bar{E}^2)^2 +$$
$$\frac{\sigma_r^2\psi_e}{\sigma_r^2 - \psi_e^2}\frac{(\sigma_r^4 + \sigma_r^2\psi_e^2)(\dot{\psi}_d - r) - 2\sigma_r\dot{\sigma}_r\psi_e^3}{(\sigma_r^2 - \psi_e^2)^2} \quad (27)$$

The designed virtual control law is given by

$$\begin{cases} a_u = \left(\dot{x}_d\cos(\psi_d) + \dot{y}_d\sin(\psi_d) - \bar{v}\sin(\psi_e) - \right. \\ \qquad \frac{2\sigma_u\dot{\sigma}_u\bar{E}^3}{(\sigma_u^4 + \sigma_u^2\bar{E}^2)} + \frac{k_1(\sigma_u^2 - \bar{E}^2)^3\bar{E}}{(\sigma_u^6 + \sigma_u^4\bar{E}^2)} + \\ \qquad \left. \frac{(\sigma_u^2 - \bar{E}^2)^2\pi}{(\sigma_u^4 + \sigma_u^2\bar{E}^2)\gamma T_u}(V_u^{1-\gamma} + V_u^{1+\gamma})\right)/\cos(\psi_e) \quad (28) \\ a_r = \dot{\psi}_d - \frac{2\sigma_r\dot{\sigma}_r\psi_e^3}{(\sigma_r^4 + \sigma_r^2\psi_e^2)} + \frac{k_2(\sigma_r^2 - \psi_e^2)}{\sigma_r^2}\psi_e + \\ \qquad \frac{(\sigma_r^2 - \psi_e^2)^2\pi}{(\sigma_r^4 + \sigma_r^2\psi_e^2)\gamma T_r}(V_r^{1-\gamma} + V_r^{1+\gamma}) \end{cases}$$

where k_1, k_2, α, β are positive constants, $0 < \alpha \leqslant 1$, $0 < \beta \leqslant 1$ and design parameters $0 < \gamma < 1$, $T_\iota > 0$, $\iota = u,r$.

To avoid "computational explosion" in taking derivations of virtual control signals, a conventional first-order filter is usually used, that is, $t_\iota\dot{a}_{f\iota} = a_{c\iota} - a_{f\iota}$, where t_ι is filter gain; $a_{c\iota}$ is an input signal of the filter; $a_{f\iota}$ is an input signal after filtering $\iota = u,r$. In this paper, an adaptive predefined-time filter is proposed to avoid "differential explosion", and an adaptive law is used to estimate unknown upper bounds of virtual control input derivatives.

Hypothesis 4: The derivative of an input signal of the adaptive predefined-time filter $(\dot{a}_{f\iota}, \iota = u,r)$ is continuous, and $|\dot{a}_{f\iota}| \leqslant \bar{\gamma}_\iota$, $\bar{\gamma}_\iota$ is an unknown positive constant.

The adaptive predefined-time filter is given by

$$T_{f\iota}\dot{a}_{f\iota} = \frac{\pi}{\gamma}\left(\xi_\iota^{1-\gamma} + \xi_\iota^{1+\gamma}\right) + T_{f\iota}\hat{\bar{\gamma}}_\iota\tanh\left(\frac{\xi_\iota}{\tau_{\iota\iota}}\right) + a_{m\iota} \quad (29)$$

$$\dot{\hat{\bar{\gamma}}}_\iota = -\frac{\pi}{\gamma T_{\gamma\iota}}\left(\frac{2-\gamma}{2}\hat{\bar{\gamma}}_\iota^{1-\gamma} + \frac{2+\gamma}{2}\hat{\bar{\gamma}}_\iota^{1+\gamma}\right) + \xi_\iota\tanh\left(\frac{\xi_\iota}{\varepsilon_{0\iota}}\right) \quad (30)$$

where

$$\iota = u,r, a_{mu} = \frac{\left(\sigma_u^4 + \sigma_u^2\bar{E}^2\right)V_u}{\left(\sigma_u^2 - \bar{E}^2\right)^2}, a_{mr} = \frac{\left(\sigma_r^4 + \sigma_r^2\psi_e^2\right)V_r}{\left(\sigma_r^2 - \psi_e^2\right)^2}$$

where $T_{f\iota}$ and $T_{\gamma\iota}$ are preset time.

Velocity and filtering errors are defined as follows:

$$u_e = a_{fu} - u, \quad r_e = a_{fr} - r$$
$$\xi_u = a_u - a_{fu}, \quad \xi_r = a_r - a_{fr} \quad (31)$$

The following Lyapunov function is constructed:

$$V_f = \frac{1}{2}\xi_u^2 + \frac{1}{2}\xi_r^2 + \frac{1}{2}\tilde{\bar{\gamma}}_u^2 + \frac{1}{2}\tilde{\bar{\gamma}}_r^2 \quad (32)$$

The derivative of Eq. (32) with respect to time is given by

$$\dot{V}_f = \xi_u\dot{\xi}_u + \xi_r\dot{\xi}_r + \tilde{\bar{\gamma}}_u\dot{\hat{\bar{\gamma}}}_u + \tilde{\bar{\gamma}}_r\dot{\hat{\bar{\gamma}}}_r =$$
$$\xi_u\left(\bar{\gamma}_u - T_{fu}^{-1}\left(\frac{\pi}{\gamma}\left(\xi_u^{1-\gamma} + \xi_u^{1+\gamma}\right) + T_{fu}\hat{\bar{\gamma}}_u\tanh\left(\frac{\xi_u}{\varepsilon_{0u}}\right) + \right.\right.$$
$$\left.\left. a_{mu}\right)\right) + \xi_r\left(\bar{\gamma}_r - T_{fr}^{-1}\left(\frac{\pi}{\gamma}\left(\xi_r^{1-\gamma} + \xi_r^{1+\gamma}\right) + \right.\right.$$
$$\left.\left. T_{fr}\hat{\bar{\gamma}}_r\tanh\left(\frac{\xi_r}{\varepsilon_{0r}}\right) + a_{mr}\right)\right) + \tilde{\bar{\gamma}}_u\dot{\hat{\bar{\gamma}}}_u + \tilde{\bar{\gamma}}_r\dot{\hat{\bar{\gamma}}}_r \leqslant$$
$$\xi_u\left(-T_{fu}^{-1}\left(\frac{\pi}{\gamma}\left(\xi_u^{1-\gamma} + \xi_u^{1+\gamma} + a_{mu}\right)\right)\right) + |\xi_u|\bar{\gamma}_u -$$
$$\xi_u\bar{\gamma}_u\tanh\left(\frac{\xi_u}{\varepsilon_{0u}}\right) + \tilde{\bar{\gamma}}_u\xi_u\tanh\left(\frac{\xi_u}{\varepsilon_{0u}}\right) +$$
$$\xi_r\left(-T_{fr}^{-1}\left(\frac{\pi}{\gamma}\left(\xi_r^{1-\gamma} + \xi_r^{1+\gamma}\right) + a_{mr}\right)\right) + |\xi_r|\bar{\gamma}_r -$$
$$\xi_r\bar{\gamma}_r\tanh\left(\frac{\xi_r}{\varepsilon_{0r}}\right) + \tilde{\bar{\gamma}}_r\xi_r\tanh\left(\frac{\xi_r}{\varepsilon_{0r}}\right) + \tilde{\bar{\gamma}}_u\dot{\hat{\bar{\gamma}}}_u + \tilde{\bar{\gamma}}_r\dot{\hat{\bar{\gamma}}}_r \leqslant$$
$$-\frac{\pi}{\gamma T_{fu}}\left(\xi_u^{2-\gamma} + \xi_u^{2+\gamma}\right) - \frac{\pi}{\gamma T_{fr}}\left(\xi_r^{2-\gamma} + \xi_r^{2+\gamma}\right) +$$
$$\tilde{\bar{\gamma}}_u(\xi_u\tanh\left(\frac{\xi_u}{\varepsilon_{0u}}\right) - \dot{\hat{\bar{\gamma}}}_u) + \tilde{\bar{\gamma}}_r\left(\xi_r\tanh\left(\frac{\xi_r}{\varepsilon_{0r}}\right) - \dot{\hat{\bar{\gamma}}}_r\right) -$$
$$\xi_u a_{mu} - \xi_r a_{mr} \quad (33)$$

According to Lemma 2, the following inequalities hold:

$$\begin{cases} \tilde{\bar{\gamma}}_\iota \hat{\bar{\gamma}}_\iota^{1-\gamma} \leqslant \dfrac{1}{2-\gamma}\left(2\bar{\gamma}_\iota^{2-\gamma} - \tilde{\bar{\gamma}}_\iota^{2-\gamma}\right) \\ \tilde{\bar{\gamma}}_\iota \hat{\bar{\gamma}}_\iota^{1+\gamma} \leqslant \dfrac{1}{2+\gamma}\left(2\bar{\gamma}_\iota^{2+\gamma} - \tilde{\bar{\gamma}}_\iota^{2+\gamma}\right) \end{cases} \qquad (34)$$

By substituting Eq. (30) into Eq. (33), based on Eq. (34), according to Lemma 4, we can transform Eq. (33) into

$$\dot{V}_f = \xi_u \dot{\xi}_u + \xi_r \dot{\xi}_r + \tilde{\bar{\gamma}}_u \dot{\tilde{\bar{\gamma}}}_u + \tilde{\bar{\gamma}}_r \dot{\tilde{\bar{\gamma}}}_r \leqslant$$

$$-\frac{\pi}{\gamma T_{fu}}\left(\left(\xi_u^2\right)^{1-\frac{\gamma}{2}} + \left(\xi_u^2\right)^{1+\frac{\gamma}{2}}\right) - \frac{\pi}{\gamma T_{fr}}\left(\left(\xi_r^2\right)^{1-\frac{\gamma}{2}} + \right.$$

$$\left.\left(\xi_r^2\right)^{1+\frac{\gamma}{2}}\right) - \frac{\pi}{\gamma T_{\gamma u}}\left(\tilde{\bar{\gamma}}_u^2\right)^{1-\frac{\gamma}{2}} - \frac{\pi}{\gamma T_{\gamma u}}\left(\tilde{\bar{\gamma}}_u^2\right)^{1+\frac{\gamma}{2}} -$$

$$\frac{\pi}{\gamma T_{\gamma r}}\left(\tilde{\bar{\gamma}}_r^2\right)^{1-\frac{\gamma}{2}} - \frac{\pi}{\gamma T_{\gamma r}}\left(\tilde{\bar{\gamma}}_r^2\right)^{1+\frac{\gamma}{2}} + \frac{\pi}{\gamma T_{\gamma u}}\left(\bar{\gamma}_u^2\right)^{1-\frac{\gamma}{2}} +$$

$$\frac{\pi}{\gamma T_{\gamma u}}\left(\bar{\gamma}_u^2\right)^{1+\frac{\gamma}{2}} + \frac{\pi}{\gamma T_{\gamma r}}\left(\bar{\gamma}_r^2\right)^{1-\frac{\gamma}{2}} + \frac{\pi}{\gamma T_{\gamma r}}\left(\bar{\gamma}_r^2\right)^{1+\frac{\gamma}{2}} -$$

$$\xi_r a_{mr} - \xi_r a_{mu} + k'_1 \bar{\iota}_1 \bar{\gamma}_u + k'_2 \bar{\iota}_2 \bar{\gamma}_r \leqslant$$

$$-\frac{\pi}{\gamma T_f}\left(V_f^{1-\frac{\gamma}{2}} + V_f^{1+\frac{\gamma}{2}}\right) + c_1 \qquad (35)$$

where $T_f = T_{fu} = T_{\gamma u} > 0$, $\iota = u, r$, $k'_1 = k'_2 = 0.278\,5$.

$$c_1 = \frac{\pi}{\gamma T_{\gamma u}}\left(\bar{\gamma}_u^2\right)^{1-\frac{\gamma}{2}} + \frac{\pi}{\gamma T_{\gamma u}}\left(\bar{\gamma}_u^2\right)^{1+\frac{\gamma}{2}} + \frac{\pi}{\gamma T_{\gamma r}}\left(\bar{\gamma}_r^2\right)^{1-\frac{\gamma}{2}} +$$

$$\frac{\pi}{\gamma T_{\gamma r}}\left(\bar{\gamma}_r^2\right)^{1+\frac{\gamma}{2}} - \xi_u a_{mu} - \xi_r a_{mr} + k'_1 \bar{\iota}_1 \bar{\gamma}_u + k'_2 \bar{\iota}_2 \bar{\gamma}_r \quad (36)$$

According to Lemma 1, all the filtered signals of the closed-loop control system will converge to a neighborhood within the predefined time ($T_{fc} = \sqrt{2}T_f$):

$$\left\{\lim_{t \to T'_c} x | V \leqslant \min\left\{\left(\frac{2\gamma T_f c_1}{\pi}\right)^{\frac{2}{2-\gamma}}, \left(\frac{2\gamma T_f c_1}{\pi}\right)^{\frac{2}{2+\gamma}}\right\}\right\} \quad (37)$$

2.2　Predefined-time SSNN

To solve the influence of unknown continuous nonlinear factors and external environmental disturbances on performance of the controller, this paper introduced an SSNN-based approximation strategy.

$$\begin{cases} F_1 = W_1^T S_1(Z_1) + \varepsilon_1(Z_1) \\ F_2 = W_2^T S_2(Z_2) + \varepsilon_2(Z_2) \end{cases} \qquad (38)$$

where $Z_1 = [u, a_u]^T$, $Z_2 = [r, a_r]^T$ are input signals of the neural network; $S_1(Z_1)$ and $S_2(Z_2)$ are central functions of the adaptive law of the neural network; $W_i = \arg\min\|f_i - W_i S_i\|$ is an ideal weight matrix; ε_i is an approximation error of the neural network.

The approximation function is designed as

$$\hat{F}_i = \hat{W}_i^T S_i(Z_i) \qquad (39)$$

The error matrix of weight is given by

$$\tilde{W}_i = W_i - \hat{W}_i \qquad (40)$$

The estimated error is given by

$$\tilde{\hbar}_i = \hbar_i - \hat{\hbar}_i \qquad (41)$$

where $\hbar_i$ is the upper bound of the estimated approximation error of the neural network. Define $\hbar_i = \max\{|\varepsilon_i|\}$, $i = 1, 2$.

Take derivations of u_e and r_e in Eq. (31):

$$\begin{cases} \dot{u}_e = \dot{a}_{fu} - \dot{u} = \\ \quad \dot{a}_{fu} - (f_1 + \zeta_u \tau_{du} - \zeta_u \Delta_u) - \xi_u \tau_u \\ \dot{r}_e = \dot{a}_{fr} - \dot{r} = \\ \quad \dot{a}_{fr} - (f_3 + \zeta_r(\tau_{dr} - \chi\tau_{dv} - \Delta_r)) - \xi_r \tau_r \end{cases} \quad (42)$$

For the unknown dynamics $F_1 = f_1 + \zeta_u \tau_{du} - \zeta_u \Delta_u$ and $F_2 = f_3 + \zeta_r(\tau_{dr} - \chi\tau_{dv}) - \zeta_r \Delta_r$, including input saturation-induced errors, unknown continuous nonlinear factors, and external environmental disturbances, an SSNN is used for approximation.

Therefore, the actual control law designed is shown in Eq. (43).

$$\begin{cases} \tau_u = \left(\dot{a}_{fu} + \dfrac{\left(\bar{\sigma}_u^4 + \bar{\sigma}_u^2 \bar{E}^2\right)V_u \cos\psi_e}{\left(\bar{\sigma}_u^2 - \bar{E}^2\right)^2} + k_u u_e - \hat{W}_1^T S_1(Z_1) + \right. \\ \quad \left. \hat{\hbar}_1 \tanh\left(\dfrac{u_e}{\bar{\lambda}_1}\right) + \dfrac{\pi}{\gamma T_{cu}}\left(u_e^{1-\gamma} + u_e^{1+\gamma}\right)\right)/\zeta_u \\ \tau_r = \left(\dot{a}_{fr} + \dfrac{\left(\bar{\sigma}_r^4 + \bar{\sigma}_r^2 \psi_e^2\right)V_r}{\left(\bar{\sigma}_r^2 - \psi_e^2\right)^2} + k_r r_e - \hat{W}_2^T S_2(Z_2) + \right. \\ \quad \left. \hat{\hbar}_2 \tanh\left(\dfrac{r_e}{\bar{\lambda}_2}\right) + \dfrac{\pi}{\gamma T_{cr}}\left(r_e^{1-\gamma} + r_e^{1+\gamma}\right)\right)/\zeta_r \end{cases} \quad (43)$$

The adaptive law is designed as

$$\begin{cases} \dot{\hat{W}}_1 = -\Gamma_1\left(S_1(Z_1)u_e + \dfrac{2\pi}{\gamma T_{wu}}\hat{W}_1\right) \\ \dot{\hat{W}}_2 = -\Gamma_2\left(S_2(Z_2)r_e + \dfrac{2\pi}{\gamma T_{wr}}\hat{W}_2\right) \end{cases} \quad (44)$$

$$\begin{cases} \dot{\hat{\hbar}}_1 = \\ \quad \Upsilon_1\left(u_e \tanh\left(\dfrac{u_e}{\bar{\lambda}_1}\right) - \dfrac{(2-\gamma)\pi}{\gamma T_{hu}}\hat{\hbar}_1^{1-\gamma} - \dfrac{(2+\gamma)\pi}{\gamma T_{hu}}\hat{\hbar}_1^{1+\gamma}\right) \\ \dot{\hat{\hbar}}_2 = \\ \quad \Upsilon_2\left(r_e \tanh\left(\dfrac{r_e}{\bar{\lambda}_2}\right) - \dfrac{(2-\gamma)\pi}{\gamma T_{hr}}\hat{\hbar}_2^{1-\gamma} - \dfrac{(2+\gamma)\pi}{\gamma T_{hr}}\hat{\hbar}_2^{1+\gamma}\right) \end{cases} \quad (45)$$

where Γ_1, Γ_2, Υ_1 and Υ_2 are adaptive law gains.

3　Analysis of predefined-time stability

Consider the following Lyapunov function:

$$V_3 = V_1 + V_f + \frac{1}{2}u_e^2 + \frac{1}{2}r_e^2 + \frac{1}{2}(\Gamma_1^{-1}\tilde{W}_1^T\tilde{W}_1) +$$

$$\frac{1}{2}(\Gamma_2^{-1}\tilde{W}_2^T\tilde{W}_2) + \frac{1}{2}(\Upsilon_1^{-1}\tilde{\hbar}_1^2) + \frac{1}{2}(\Upsilon_2^{-1}\tilde{\hbar}_2^2) \qquad (46)$$

The derivative of V_3 is given by

$$\dot{V}_3 = \dot{V}_1 + \dot{V}_f + u_e\dot{u}_e + r_e\dot{r}_e + \Gamma_1^{-1}\tilde{\boldsymbol{W}}_1^T\dot{\hat{\boldsymbol{W}}}_1 + \Gamma_2^{-1}\tilde{\boldsymbol{W}}_2^T\dot{\hat{\boldsymbol{W}}}_2 + \Upsilon_1^{-1}\tilde{\hbar}_1\dot{\hat{\hbar}}_1 + \Upsilon_2^{-1}\tilde{\hbar}_2\dot{\hat{\hbar}}_2 \leqslant$$
$$-k_1\bar{E}^2 - k_2\psi_e^2 - \frac{\pi}{\gamma T_u}\left(\left(V_u^2\right)^{1-\frac{\gamma}{2}} + \left(V_u^2\right)^{1+\frac{\gamma}{2}}\right) - k_u u_e^2 - k_r r_e^2 - \frac{\pi}{\gamma T_r}\left(\left(V_r^2\right)^{1-\frac{\gamma}{2}} + \left(V_r^2\right)^{1+\frac{\gamma}{2}}\right) -$$
$$\frac{\pi}{\gamma T_{cu}}\left(u_e^{1-\frac{\gamma}{2}} + u_e^{1+\frac{\gamma}{2}}\right) - \frac{\pi}{\gamma T_{cr}}\left(r_e^{1-\frac{\gamma}{2}} + r_e^{1+\frac{\gamma}{2}}\right) - \frac{\pi}{\gamma T_{fu}}\left(\left(\xi_u^2\right)^{1-\frac{\gamma}{2}} + \left(\xi_u^2\right)^{1+\frac{\gamma}{2}}\right) - \frac{\pi}{\gamma T_{fr}}\left(\left(\xi_r^2\right)^{1-\frac{\gamma}{2}} + \left(\xi_r^2\right)^{1+\frac{\gamma}{2}}\right) -$$
$$\frac{\pi}{\gamma T_{\gamma u}}\left(\tilde{\bar{\gamma}}_u^2\right)^{1-\frac{\gamma}{2}} - \frac{\pi}{\gamma T_{\gamma u}}\left(\tilde{\bar{\gamma}}_u^2\right)^{1+\frac{\gamma}{2}} - \frac{\pi}{\gamma T_{\gamma r}}\left(\tilde{\bar{\gamma}}_r^2\right)^{1-\frac{\gamma}{2}} - \frac{\pi}{\gamma T_{\gamma r}}\left(\tilde{\bar{\gamma}}_r^2\right)^{1+\frac{\gamma}{2}} - u_e\tilde{\boldsymbol{W}}_1^T\boldsymbol{S}_1(\boldsymbol{Z}_1) - r_e\tilde{\boldsymbol{W}}_2^T\boldsymbol{S}_2(\boldsymbol{Z}_2) +$$
$$\left(|u_e|\hbar_1 - u_e\hat{\hbar}_1\tanh\left(\frac{u_e}{\lambda_1}\right)\right) + \left(|r_e|\hbar_2 - r_e\hat{\hbar}_2\tanh\left(\frac{r_e}{\lambda_2}\right)\right) - \Gamma_1^{-1}\tilde{\boldsymbol{W}}_1^T\dot{\hat{\boldsymbol{W}}}_1 - \Gamma_2^{-1}\tilde{\boldsymbol{W}}_2^T\dot{\hat{\boldsymbol{W}}}_2 - \Upsilon_1^{-1}\tilde{\hbar}_1\dot{\hat{\hbar}}_1 - \Upsilon_2^{-1}\tilde{\hbar}_2\dot{\hat{\hbar}}_2 +$$
$$\frac{\pi}{\gamma T_{\gamma u}}(\bar{\gamma}_u^2)^{1-\frac{\gamma}{2}} + \frac{\pi}{\gamma T_{\gamma u}}(\bar{\gamma}_u^2)^{1+\frac{\gamma}{2}} + \frac{\pi}{\gamma T_{\gamma r}}(\bar{\gamma}_r^2)^{1-\frac{\gamma}{2}} + \frac{\pi}{\gamma T_{\gamma r}}(\bar{\gamma}_r^2)^{1+\frac{\gamma}{2}} + k_1'\lambda_1\bar{\gamma}_u + k_2'\lambda_2\bar{\gamma}_r \tag{47}$$

According to Lemma 4, based on Eq. (41), Eq. (47) can be transformed into

$$\dot{V}_3 \leqslant -k_1\bar{E}^2 - k_2\psi_e^2 - k_u u_e^2 - k_r r_e^2 - \frac{\pi}{\gamma T_u}\left(\left(V_u^2\right)^{1-\frac{\gamma}{2}} + \left(V_u^2\right)^{1+\frac{\gamma}{2}}\right) - \frac{\pi}{\gamma T_r}\left(\left(V_r^2\right)^{1-\frac{\gamma}{2}} + \left(V_r^2\right)^{1+\frac{\gamma}{2}}\right) -$$
$$\frac{\pi}{\gamma T_{cu}}\left(u_e^{1-\frac{\gamma}{2}} + u_e^{1+\frac{\gamma}{2}}\right) - \frac{\pi}{\gamma T_{cr}}\left(r_e^{1-\frac{\gamma}{2}} + r_e^{1+\frac{\gamma}{2}}\right) - \frac{\pi}{\gamma T_{fu}}\left(\left(\xi_u^2\right)^{1-\frac{\gamma}{2}} + \left(\xi_u^2\right)^{1+\frac{\gamma}{2}}\right) - \frac{\pi}{\gamma T_{fr}}\left(\left(\xi_r^2\right)^{1-\frac{\gamma}{2}} + \left(\xi_r^2\right)^{1+\frac{\gamma}{2}}\right) -$$
$$\frac{\pi}{\gamma T_{\gamma u}}\left(\tilde{\bar{\gamma}}_u^2\right)^{1-\frac{\gamma}{2}} - \frac{\pi}{\gamma T_{\gamma u}}\left(\tilde{\bar{\gamma}}_u^2\right)^{1+\frac{\gamma}{2}} - \frac{\pi}{\gamma T_{\gamma r}}\left(\tilde{\bar{\gamma}}_r^2\right)^{1-\frac{\gamma}{2}} - \frac{\pi}{\gamma T_{\gamma r}}\left(\tilde{\bar{\gamma}}_r^2\right)^{1+\frac{\gamma}{2}} + \Gamma_1^{-1}\tilde{\boldsymbol{W}}_1^T(-\dot{\hat{\boldsymbol{W}}}_1 - \Gamma_1 u_e\boldsymbol{S}_1(\boldsymbol{Z}_1)) +$$
$$\Gamma_2^{-1}\tilde{\boldsymbol{W}}_2^T(-\dot{\hat{\boldsymbol{W}}}_2 - \Gamma_2 r_e\boldsymbol{S}_2(\boldsymbol{Z}_2)) + \Upsilon_1^{-1}\tilde{\hbar}_1\left(\Upsilon_1 u_e\tanh\left(\frac{u_e}{\lambda_1}\right) - \dot{\hat{\hbar}}_1\right) + \Upsilon_2^{-1}\tilde{\hbar}_2\left(\Upsilon_2 r_e\tanh\left(\frac{r_e}{\lambda_2}\right) - \dot{\hat{\hbar}}_2\right) +$$
$$\frac{\pi}{\gamma T_{\gamma u}}(\bar{\gamma}_u^2)^{1-\frac{\gamma}{2}} + \frac{\pi}{\gamma T_{\gamma u}}(\bar{\gamma}_u^2)^{1+\frac{\gamma}{2}} + \frac{\pi}{\gamma T_{\gamma r}}(\bar{\gamma}_r^2)^{1-\frac{\gamma}{2}} + \frac{\pi}{\gamma T_{\gamma r}}(\bar{\gamma}_r^2)^{1+\frac{\gamma}{2}} + k_1'\lambda_1\bar{\gamma}_u + k_2'\lambda_2\bar{\gamma}_r + k_3'\lambda_3|\hbar_1| + k_4'\lambda_4|\hbar_2| \tag{48}$$

Substitute Eqs. (44) and (45) into Eq. (48):

$$\dot{V}_3 \leqslant -k_1\bar{E}^2 - k_2\psi_e^2 - k_u u_e^2 - k_r r_e^2 - \frac{\pi}{\gamma T_u}\left(\left(V_u^2\right)^{1-\frac{\gamma}{2}} + \left(V_u^2\right)^{1+\frac{\gamma}{2}}\right) - \frac{\pi}{\gamma T_r}\left(\left(V_r^2\right)^{1-\frac{\gamma}{2}} + \left(V_r^2\right)^{1+\frac{\gamma}{2}}\right) -$$
$$\frac{\pi}{\gamma T_{cu}}\left(u_e^{1-\frac{\gamma}{2}} + u_e^{1+\frac{\gamma}{2}}\right) - \frac{\pi}{\gamma T_{cr}}\left(r_e^{1-\frac{\gamma}{2}} + r_e^{1+\frac{\gamma}{2}}\right) - \frac{\pi}{\gamma T_{fu}}\left(\left(\xi_u^2\right)^{1-\frac{\gamma}{2}} + \left(\xi_u^2\right)^{1+\frac{\gamma}{2}}\right) -$$
$$\frac{\pi}{\gamma T_{fr}}\left(\left(\xi_r^2\right)^{1-\frac{\gamma}{2}} + \left(\xi_r^2\right)^{1+\frac{\gamma}{2}}\right) - \frac{\pi}{\gamma T_{\gamma u}}\left(\tilde{\bar{\gamma}}_u^2\right)^{1-\frac{\gamma}{2}} - \frac{\pi}{\gamma T_{\gamma u}}\left(\tilde{\bar{\gamma}}_u^2\right)^{1+\frac{\gamma}{2}} - \frac{\pi}{\gamma T_{\gamma r}}\left(\tilde{\bar{\gamma}}_r^2\right)^{1-\frac{\gamma}{2}} - \frac{\pi}{\gamma T_{\gamma r}}\left(\tilde{\bar{\gamma}}_r^2\right)^{1+\frac{\gamma}{2}} -$$
$$\frac{\pi}{\gamma T_{wu}}\tilde{\boldsymbol{W}}_1^T\tilde{\boldsymbol{W}}_1 + \frac{\pi}{\gamma T_{wu}}\tilde{\boldsymbol{W}}_1^T\boldsymbol{W}_1 - \frac{\pi}{\gamma T_{wr}}\tilde{\boldsymbol{W}}_2^T\tilde{\boldsymbol{W}}_2 + \frac{\pi}{\gamma T_{wr}}\tilde{\boldsymbol{W}}_2^T\boldsymbol{W}_2 + \frac{\pi}{\gamma T_{hu}}\tilde{\hbar}_1\left(\hat{\hbar}_1^{1-\gamma} + \hat{\hbar}_1^{1+\gamma}\right) + \frac{\pi}{\gamma T_{hr}}\tilde{\hbar}_2\left(\hat{\hbar}_2^{1-\gamma} + \hat{\hbar}_2^{1+\gamma}\right) +$$
$$\frac{\pi}{\gamma T_{\gamma u}}(\bar{\gamma}_u^2)^{1-\frac{\gamma}{2}} + \frac{\pi}{\gamma T_{\gamma u}}(\bar{\gamma}_u^2)^{1+\frac{\gamma}{2}} + \frac{\pi}{\gamma T_{\gamma r}}(\bar{\gamma}_r^2)^{1-\frac{\gamma}{2}} + \frac{\pi}{\gamma T_{\gamma r}}(\bar{\gamma}_r^2)^{1+\frac{\gamma}{2}} + k_1'\lambda_1\bar{\gamma}_u + k_2'\lambda_2\bar{\gamma}_r + k_3'\lambda_3|\hbar_1| + k_4'\lambda_4|\hbar_2| \tag{49}$$

According to Lemma 2, the following inequalities are satisfied:

$$\begin{cases} \tilde{\hbar}_\iota\hat{\hbar}_\iota^{1-\gamma} \leqslant \dfrac{1}{2-\gamma}(2\hbar_\iota^{2-\gamma} - \tilde{\hbar}_\iota^{2-\gamma}) \\ \tilde{\hbar}_\iota\hat{\hbar}_\iota^{1+\gamma} \leqslant \dfrac{1}{2+\gamma}(2\hbar_\iota^{2+\gamma} - \tilde{\hbar}_\iota^{2+\gamma}) \end{cases} \tag{50}$$

According to Young's inequality, the following

$$\begin{cases} \dfrac{2\pi}{\gamma T_{wu}}\tilde{\boldsymbol{W}}_1^T\boldsymbol{W}_1 \leqslant \dfrac{\pi}{\gamma T_{wu}}\tilde{\boldsymbol{W}}_1^T\tilde{\boldsymbol{W}}_1 + \dfrac{\pi}{\gamma T_{wu}}\boldsymbol{W}_1^T\boldsymbol{W}_1 \\ \dfrac{2\pi}{\gamma T_{wr}}\tilde{\boldsymbol{W}}_2^T\boldsymbol{W}_2 \leqslant \dfrac{\pi}{\gamma T_{wr}}\tilde{\boldsymbol{W}}_2^T\tilde{\boldsymbol{W}}_2 + \dfrac{\pi}{\gamma T_{wr}}\boldsymbol{W}_2^T\boldsymbol{W}_2 \end{cases} \tag{51}$$

Then, Eq. (49) can be transformed into

$$\dot{V}_3 \leqslant -k_1\bar{E}^2 - k_2\psi_e^2 - k_u u_e^2 - k_r r_e^2 - \frac{\pi}{\gamma T_u}\left(\left(V_u^2\right)^{1-\frac{\gamma}{2}} + \left(V_u^2\right)^{1+\frac{\gamma}{2}}\right) - \frac{\pi}{\gamma T_r}\left(\left(V_r^2\right)^{1-\frac{\gamma}{2}} + \left(V_r^2\right)^{1+\frac{\gamma}{2}}\right) -$$
$$\frac{\pi}{\gamma T_{cu}}\left(u_e^{1-\frac{\gamma}{2}} + u_e^{1+\frac{\gamma}{2}}\right) - \frac{\pi}{\gamma T_{cr}}\left(r_e^{1-\frac{\gamma}{2}} + r_e^{1+\frac{\gamma}{2}}\right) - \frac{\pi}{\gamma T_{fu}}\left(\left(\xi_u^2\right)^{1-\frac{\gamma}{2}} + \left(\xi_u^2\right)^{1+\frac{\gamma}{2}}\right) - \frac{\pi}{\gamma T_{fr}}\left(\left(\xi_r^2\right)^{1-\frac{\gamma}{2}} + \left(\xi_r^2\right)^{1+\frac{\gamma}{2}}\right) -$$
$$\frac{\pi}{\gamma T_{\gamma u}}\left(\tilde{\bar{\gamma}}_u^2\right)^{1-\frac{\gamma}{2}} - \frac{\pi}{\gamma T_{\gamma u}}\left(\tilde{\bar{\gamma}}_u^2\right)^{1+\frac{\gamma}{2}} - \frac{\pi}{\gamma T_{\gamma r}}\left(\tilde{\bar{\gamma}}_r^2\right)^{1-\frac{\gamma}{2}} - \frac{\pi}{\gamma T_{\gamma r}}\left(\tilde{\bar{\gamma}}_r^2\right)^{1+\frac{\gamma}{2}} - \frac{\pi}{\gamma T_{wu}}\tilde{\boldsymbol{W}}_1^T\tilde{\boldsymbol{W}}_1 - \frac{\pi}{\gamma T_{wr}}\tilde{\boldsymbol{W}}_2^T\tilde{\boldsymbol{W}}_2 -$$
$$\frac{\pi}{\gamma T_{hu}}\left(\left(\tilde{\hbar}_1^2\right)^{1-\frac{\gamma}{2}} + \left(\tilde{\hbar}_1^2\right)^{1+\frac{\gamma}{2}}\right) - \frac{\pi}{\gamma T_{hr}}\left(\left(\tilde{\hbar}_2^2\right)^{1-\frac{\gamma}{2}} + \left(\tilde{\hbar}_2^2\right)^{1+\frac{\gamma}{2}}\right) + \frac{2\pi}{\gamma T_{fu}}(\bar{\gamma}_u^2)^{1-\frac{\gamma}{2}} + \frac{2\pi}{\gamma T_{fu}}(\bar{\gamma}_u^2)^{1+\frac{\gamma}{2}} + \frac{2\pi}{\gamma T_{fr}}(\bar{\gamma}_r^2)^{1-\frac{\gamma}{2}} +$$

$$\frac{2\pi}{\gamma T_{\mathrm{fr}}}(\bar{\gamma}_r^2)^{1+\frac{\gamma}{2}} + k_1'\tau_1\bar{\gamma}_u + k_2'\tau_2\bar{\gamma}_r + k_3'\tau_3|\hbar_1| + k_4'\tau_4|\hbar_2| + \frac{2\pi}{\gamma T_{\mathrm{hu}}}\left(\hbar_1^{2-\gamma} + \hbar_1^{2+\gamma}\right) + \frac{2\pi}{\gamma T_{\mathrm{hr}}}\left(\hbar_2^{2-\gamma} + \hbar_2^{2+\gamma}\right) +$$

$$\frac{\pi}{2\gamma T_{\mathrm{wu}}}W_1^{\mathrm{T}}W_1 + \frac{\pi}{2\gamma T_{\mathrm{wr}}}W_2^{\mathrm{T}}W_2 \leqslant$$

$$-\frac{\pi}{\gamma T_u}V_u^2 - \frac{\pi}{\gamma T_r}V_r^2 - \frac{\pi}{\gamma T_{\mathrm{fu}}}\xi_u^2 - \frac{\pi}{\gamma T_{\mathrm{fr}}}\xi_r^2 - \frac{\pi}{\gamma T_{\mathrm{fu}}}\tilde{\bar{\gamma}}_u^2 - \frac{\pi}{\gamma T_{\mathrm{fr}}}\tilde{\bar{\gamma}}_r^2 - k_u u_{\mathrm{e}}^2 - k_r r_{\mathrm{e}}^2 - \frac{\pi}{\gamma T_{\mathrm{wu}}}\tilde{W}_1^{\mathrm{T}}\tilde{W}_1 - \frac{\pi}{\gamma T_{\mathrm{wr}}}\tilde{W}_2^{\mathrm{T}}\tilde{W}_2 -$$

$$\frac{\pi}{\gamma T_{\mathrm{hu}}}\tilde{\hbar}_1^2 - \frac{\pi}{\gamma T_{\mathrm{hr}}}\tilde{\hbar}_2^2 + \frac{2\pi}{\gamma T_{\mathrm{fu}}}(\bar{\gamma}_u^2)^{1-\frac{\gamma}{2}} + \frac{2\pi}{\gamma T_{\mathrm{fu}}}(\bar{\gamma}_u^2)^{1+\frac{\gamma}{2}} + \frac{2\pi}{\gamma T_{\mathrm{fr}}}(\bar{\gamma}_r^2)^{1-\frac{\gamma}{2}} + \frac{2\pi}{\gamma T_{\mathrm{fr}}}(\bar{\gamma}_r^2)^{1+\frac{\gamma}{2}} + k_1'\tau_1\bar{\gamma}_u + k_2'\tau_2\bar{\gamma}_r +$$

$$k_3'\tau_3|\hbar_1| + k_4'\tau_4|\hbar_2| + \frac{2\pi}{\gamma T_{\mathrm{hu}}}\left(\hbar_1^{2-\gamma} + \hbar_1^{2+\gamma}\right) + \frac{2\pi}{\gamma T_{\mathrm{hr}}}\left(\hbar_2^{2-\gamma} + \hbar_2^{2+\gamma}\right) + \frac{\pi}{\gamma T_{\mathrm{wu}}}W_1^{\mathrm{T}}W_1 + \frac{\pi}{\gamma T_{\mathrm{wr}}}W_2^{\mathrm{T}}W_2 \leqslant \rho_0 V_3 + \varDelta_0 \quad (52)$$

Both sides of Eq. (52) are integrated simultaneously and the following inequality is met:

$$0 \leqslant V_3 \leqslant \left(V_3(0) - \frac{\varDelta_0}{\rho_0}\right)\mathrm{e}^{-k_0 t} + \frac{\varDelta_0}{\rho_0} \quad (53)$$

V_3 is obviously bounded, which means that tracking errors are uniformly bounded. Therefore, we further assume that there is always a positive constant $\mathbb{V}_{\mathrm{M}i}$ satisfying the following inequality: $\tilde{W}_i^{\mathrm{T}}\tilde{W}_i \leqslant \mathbb{V}_{\mathrm{M}i}$, $i = 1, 2$.

$$\dot{V}_3 \leqslant -k_1\bar{E}^2 - k_2\psi_{\mathrm{e}}^2 - k_u u_{\mathrm{e}}^2 - k_r r_{\mathrm{e}}^2 - \frac{\pi}{\gamma T_u}\left(\left(V_u^2\right)^{1-\frac{\gamma}{2}} + \left(V_u^2\right)^{1+\frac{\gamma}{2}}\right) - \frac{\pi}{\gamma T_r}\left(\left(V_r^2\right)^{1-\frac{\gamma}{2}} + \left(V_r^2\right)^{1+\frac{\gamma}{2}}\right) - \frac{\pi}{\gamma T_{\mathrm{cu}}}\left(u_{\mathrm{e}}^{1-\frac{\gamma}{2}} + u_{\mathrm{e}}^{1+\frac{\gamma}{2}}\right) -$$

$$\frac{\pi}{\gamma T_{\mathrm{cr}}}\left(r_{\mathrm{e}}^{1-\frac{\gamma}{2}} + r_{\mathrm{e}}^{1+\frac{\gamma}{2}}\right) - \frac{\pi}{\gamma T_{\mathrm{fu}}}\left(\left(\xi_u^2\right)^{1-\frac{\gamma}{2}} + \left(\xi_u^2\right)^{1+\frac{\gamma}{2}}\right) - \frac{\pi}{\gamma T_{\mathrm{fr}}}\left(\left(\xi_r^2\right)^{1-\frac{\gamma}{2}} + \left(\xi_r^2\right)^{1+\frac{\gamma}{2}}\right) - \frac{\pi}{\gamma T_{\gamma u}}\left(\tilde{\bar{\gamma}}_u^2\right)^{1-\frac{\gamma}{2}} - \frac{\pi}{\gamma T_{\gamma u}}\left(\tilde{\bar{\gamma}}_u^2\right)^{1+\frac{\gamma}{2}} -$$

$$\frac{\pi}{\gamma T_{\gamma r}}\left(\tilde{\bar{\gamma}}_r^2\right)^{1-\frac{\gamma}{2}} - \frac{\pi}{\gamma T_{\gamma r}}\left(\tilde{\bar{\gamma}}_r^2\right)^{1+\frac{\gamma}{2}} - \frac{\pi}{\gamma T_{\mathrm{wu}}}\tilde{W}_1^{\mathrm{T}}\tilde{W}_1 - \frac{\pi}{\gamma T_{\mathrm{wr}}}\tilde{W}_2^{\mathrm{T}}\tilde{W}_2 - \frac{\pi}{\gamma T_{\mathrm{wu}}}\left(\left(\tilde{W}_1^{\mathrm{T}}\tilde{W}_1\right)^{1-\frac{\gamma}{2}} + \left(\tilde{W}_1^{\mathrm{T}}\tilde{W}_1\right)^{1+\frac{\gamma}{2}}\right) -$$

$$\frac{\pi}{\gamma T_{\mathrm{wr}}}\left(\left(\tilde{W}_2^{\mathrm{T}}\tilde{W}_2\right)^{1-\frac{\gamma}{2}} + \left(\tilde{W}_2^{\mathrm{T}}\tilde{W}_2\right)^{1+\frac{\gamma}{2}}\right) + \frac{\pi}{\gamma T_{\mathrm{wu}}}\left(\tilde{W}_1^{\mathrm{T}}\tilde{W}_1\right)^{1-\frac{\gamma}{2}} + \frac{\pi}{\gamma T_{\mathrm{wu}}}\left(\tilde{W}_1^{\mathrm{T}}\tilde{W}_1\right)^{1+\frac{\gamma}{2}} + \frac{\pi}{\gamma T_{\mathrm{wr}}}\left(\tilde{W}_2^{\mathrm{T}}\tilde{W}_2\right)^{1-\frac{\gamma}{2}} + \frac{\pi}{\gamma T_{\mathrm{wr}}}\left(\tilde{W}_2^{\mathrm{T}}\tilde{W}_2\right)^{1+\frac{\gamma}{2}} -$$

$$\frac{\pi}{\gamma T_{\mathrm{hu}}}\left(\left(\tilde{\hbar}_1^2\right)^{1-\frac{\gamma}{2}} + \left(\tilde{\hbar}_1^2\right)^{1+\frac{\gamma}{2}}\right) - \frac{\pi}{\gamma T_{\mathrm{hr}}}\left(\left(\tilde{\hbar}_2^2\right)^{1-\frac{\gamma}{2}} + \left(\tilde{\hbar}_2^2\right)^{1+\frac{\gamma}{2}}\right) + \frac{2\pi}{\gamma T_{\mathrm{fu}}}(\bar{\gamma}_u^2)^{1-\frac{\gamma}{2}} + \frac{2\pi}{\gamma T_{\mathrm{fu}}}(\bar{\gamma}_u^2)^{1+\frac{\gamma}{2}} + \frac{2\pi}{\gamma T_{\mathrm{fr}}}(\bar{\gamma}_r^2)^{1-\frac{\gamma}{2}} + \frac{2\pi}{\gamma T_{\mathrm{fr}}}(\bar{\gamma}_r^2)^{1+\frac{\gamma}{2}} +$$

$$k_1'\tau_1\bar{\gamma}_u + k_2'\tau_2\bar{\gamma}_r + k_3'\tau_3|\hbar_1| + k_4'\tau_4|\hbar_2| + \frac{2\pi}{\gamma T_{\mathrm{hu}}}\left(\hbar_1^{2-\gamma} + \hbar_1^{2+\gamma}\right) + \frac{2\pi}{\gamma T_{\mathrm{hr}}}\left(\hbar_2^{2-\gamma} + \hbar_2^{2+\gamma}\right) + \frac{\pi}{2\gamma T_{\mathrm{wu}}}W_1^{\mathrm{T}}W_1 + \frac{\pi}{2\gamma T_{\mathrm{wr}}}W_2^{\mathrm{T}}W_2 \quad (54)$$

In fact, if there is $a > 0$ satisfying the following inequality

$$a^{1-\frac{\gamma}{2}} - a \leqslant \left(\frac{2-\gamma}{2}\right)^{\frac{2-\gamma}{\gamma}} - \left(\frac{2-\gamma}{2}\right)^{\frac{2}{\gamma}} = \mathbb{V}_1 \quad (55)$$

Eq. (54) realizes asymptotic convergence of the closed-loop system. Further considering the predefined-time convergence of the closed-loop system, based on Eq. (55), we can rewrite Eq. (54) as

$$\dot{V}_3 \leqslant -k_1\bar{E}^2 - k_2\psi_{\mathrm{e}}^2 - k_u u_{\mathrm{e}}^2 - k_r r_{\mathrm{e}}^2 - \frac{\pi}{\gamma T_u}\left(\left(V_u^2\right)^{1-\frac{\gamma}{2}} + \left(V_u^2\right)^{1+\frac{\gamma}{2}}\right) - \frac{\pi}{\gamma T_r}\left(\left(V_r^2\right)^{1-\frac{\gamma}{2}} + \left(V_r^2\right)^{1+\frac{\gamma}{2}}\right) - \frac{\pi}{\gamma T_{\mathrm{cu}}}\left(u_{\mathrm{e}}^{1-\frac{\gamma}{2}} + u_{\mathrm{e}}^{1+\frac{\gamma}{2}}\right) -$$

$$\frac{\pi}{\gamma T_{\mathrm{cr}}}\left(r_{\mathrm{e}}^{1-\frac{\gamma}{2}} + r_{\mathrm{e}}^{1+\frac{\gamma}{2}}\right) - \frac{\pi}{\gamma T_{\mathrm{fu}}}\left(\left(\xi_u^2\right)^{1-\frac{\gamma}{2}} + \left(\xi_u^2\right)^{1+\frac{\gamma}{2}}\right) - \frac{\pi}{\gamma T_{\mathrm{fr}}}\left(\left(\xi_r^2\right)^{1-\frac{\gamma}{2}} + \left(\xi_r^2\right)^{1+\frac{\gamma}{2}}\right) - \frac{\pi}{\gamma T_{\gamma u}}\left(\tilde{\bar{\gamma}}_u^2\right)^{1-\frac{\gamma}{2}} - \frac{\pi}{\gamma T_{\gamma u}}\left(\tilde{\bar{\gamma}}_u^2\right)^{1+\frac{\gamma}{2}} -$$

$$\frac{\pi}{\gamma T_{\gamma r}}\left(\tilde{\bar{\gamma}}_r^2\right)^{1-\frac{\gamma}{2}} - \frac{\pi}{\gamma T_{\gamma r}}\left(\tilde{\bar{\gamma}}_r^2\right)^{1+\frac{\gamma}{2}} - \frac{\pi}{\gamma T_{\mathrm{wu}}}\left(\left(\tilde{W}_1^{\mathrm{T}}\tilde{W}_1\right)^{1-\frac{\gamma}{2}} + \left(\tilde{W}_1^{\mathrm{T}}\tilde{W}_1\right)^{1+\frac{\gamma}{2}}\right) - \frac{\pi}{\gamma T_{\mathrm{wr}}}\left(\left(\tilde{W}_2^{\mathrm{T}}\tilde{W}_2\right)^{1-\frac{\gamma}{2}} + \left(\tilde{W}_2^{\mathrm{T}}\tilde{W}_2\right)^{1+\frac{\gamma}{2}}\right) -$$

$$\frac{\pi}{\gamma T_{\mathrm{hu}}}\left(\left(\tilde{\hbar}_1^2\right)^{1-\frac{\gamma}{2}} + \left(\tilde{\hbar}_1^2\right)^{1+\frac{\gamma}{2}}\right) - \frac{\pi}{\gamma T_{\mathrm{hr}}}\left(\left(\tilde{\hbar}_2^2\right)^{1-\frac{\gamma}{2}} + \left(\tilde{\hbar}_2^2\right)^{1+\frac{\gamma}{2}}\right) + \frac{2\pi}{\gamma T_{\gamma u}}(\bar{\gamma}_u^2)^{1-\frac{\gamma}{2}} + \frac{2\pi}{\gamma T_{\gamma u}}(\bar{\gamma}_u^2)^{1+\frac{\gamma}{2}} + \frac{2\pi}{\gamma T_{\gamma r}}(\bar{\gamma}_r^2)^{1-\frac{\gamma}{2}} +$$

$$\frac{2\pi}{\gamma T_{\gamma r}}(\bar{\gamma}_r^2)^{1+\frac{\gamma}{2}} + k_1'\tau_1\bar{\gamma}_u + k_2'\tau_2\bar{\gamma}_r + k_3'\tau_3|\hbar_1| + k_4'\tau_4|\hbar_2| + \frac{2\pi}{\gamma T_{\mathrm{hu}}}\left(\hbar_1^{2-\gamma} + \hbar_1^{2+\gamma}\right) + \frac{2\pi}{\gamma T_{\mathrm{hr}}}\left(\hbar_2^{2-\gamma} + \hbar_2^{2+\gamma}\right) +$$

$$\frac{\pi}{\gamma T_{\mathrm{wu}}}W_1^{\mathrm{T}}W_1 + \frac{\pi}{\gamma T_{\mathrm{wr}}}W_2^{\mathrm{T}}W_2 + \mathbb{V}_{\mathrm{M}1} + \mathbb{V}_{\mathrm{M}2} + \mathbb{V}_1 \leqslant -\frac{\pi}{\gamma T_{\mathrm{c}}}\left(V_3^{1-\frac{\gamma}{2}} + V_3^{1+\frac{\gamma}{2}}\right) + \vartheta \quad (56)$$

where

$$
\begin{cases}
T_c = \\
\max\{T_u, T_r, T_{fu}, T_{fr}, T_{\gamma u}, T_{\gamma r}, T_{wu}, T_{wr}, T_{hu}, T_{hr}\} \\
\vartheta = \dfrac{2\pi}{\gamma T_{\gamma u}}(\bar{\gamma}_u^2)^{1-\frac{\gamma}{2}} + \dfrac{2\pi}{\gamma T_{\gamma u}}(\bar{\gamma}_u^2)^{1+\frac{\gamma}{2}} + \dfrac{2\pi}{\gamma T_{\gamma r}}(\bar{\gamma}_r^2)^{1-\frac{\gamma}{2}} + \\
\quad \dfrac{2\pi}{\gamma T_{\gamma r}}(\bar{\gamma}_r^2)^{1+\frac{\gamma}{2}} + k_1'\tau_1\bar{\gamma}_u + k_2'\tau_2\bar{\gamma}_r + k_3'\tau_3|\hbar_1| + \\
\quad k_4'\tau_4|\hbar_2| + \dfrac{2\pi}{\gamma T_{hu}}\left(\hbar_1^{2-\gamma} + \hbar_1^{2+\gamma}\right) + \\
\quad \dfrac{2\pi}{\gamma T_{hr}}\left(\hbar_2^{2-\gamma} + \hbar_2^{2+\gamma}\right) + \dfrac{\pi}{\gamma T_{wu}}W_1^{\mathrm{T}}W_1 + \\
\quad \dfrac{\pi}{\gamma T_{wr}}W_2^{\mathrm{T}}W_2 + \mathbb{V}_{M1} + \mathbb{V}_{M2} + \mathbb{V}_1
\end{cases}
\tag{57}
$$

According to Lemma 1, in the control system, all signals converge to a regional set near the origin within a predefined time.

$$
\left\{\lim_{t\to T_c'} x \Big| V \leqslant \min\left\{\left(\dfrac{2\gamma T_c \vartheta}{\pi}\right)^{\frac{2}{2-\gamma}}, \left(\dfrac{2\gamma T_c \vartheta}{\pi}\right)^{\frac{2}{2+\gamma}}\right\}\right\}
$$

The convergence time satisfies

$$
T_N \leqslant T_{\max} = \sqrt{2}T_c \tag{58}
$$

4 Simulation results

A desired circular trajectory was given by

$$
\begin{cases}
x_d = 80 + 50\sin(0.05t) \\
y_d = 80 - 50\cos(0.05t)
\end{cases}
\tag{59}
$$

Under the circular trajectory, four initial states were selected as follows:

State 1: $\eta_0 = [75, 28, 0]^{\mathrm{T}}$, $v_0 = [0, 0, 0]^{\mathrm{T}}$.

State 2: $\eta_0 = [77, 27, 0.2]^{\mathrm{T}}$, $v_0 = [0.01, 0, 0]^{\mathrm{T}}$.

State 3: $\eta_0 = [76, 33, 0.1]^{\mathrm{T}}$, $v_0 = [0.02, -0.01, 0]^{\mathrm{T}}$.

State 4: $\eta_0 = [83, 34, -0.8]^{\mathrm{T}}$, $v_0 = [0.02, 0, 0.01]^{\mathrm{T}}$.

Asymmetric input saturation was set to

$$
\tau_u^+ = 500 \text{ N}, \ \tau_u^- = -400 \text{ N}
$$

$$
\tau_r^+ = 50 \text{ N}\cdot\text{m}, \ \tau_r^- = -40 \text{ N}\cdot\text{m}
$$

External time-varying environment disturbances were given by

$$
\begin{cases}
\tau_{du} = -14 + 6\sin(0.5t)\cos(0.5t) - \\
\quad 8\sin(0.5t)\sin(t) - 4\cos(0.5t) \\
\tau_{dv} = 5\sin(0.1t) + 2\cos(0.3t) \\
\tau_{dr} = 6\cos(0.3t)\sin(1.1t) + 3\sin(0.5t) + 5\cos(0.2t)
\end{cases}
\tag{60}
$$

Table 1 lists dynamics model parameters of the selected USV in the simulation, and control parameters set in this paper are shown in Table 2. Predefined-time parameters are as follows: $\gamma = 0.35$, $T_\iota = 6$ s, $T_{c\iota} = 6$ s, $T_{w\iota} = 6$ s, $T_{h\iota} = 6$ s, $T_{f\iota} = 6$ s, $T_{\gamma\iota} = 6$ s, $\iota = u, r$.

Parameters of the SSNN were as follows: $\Gamma_1 = 250$, $\Gamma_2 = 250$, and initial values of the estimations of SSNN weight $\hat{W}_1$ and $\hat{W}_2$ were $\hat{W}_1 = \hat{W}_2 = 0$. The initial number of neurons was $N = 41$. Centers of the SSNN's Gaussian function were uniformly distributed within $[-8, 8]$, with a breadth of 0.85. The split threshold was $\Upsilon_s = 0.8$ and the decay threshold was $\Upsilon_d = 0.1$, and $p_d = 0.3$. For performance comparison between SSNN and RBFNNs, RBFNNs adopted the same parameters as the SSNN did.

Fig. 4 illustrates trajectory tracking effect in the case of different initial positions of the USV. Figs. 5−6 illustrate corresponding tracking errors. According to Figs. 4−6, despite different initial positions, the designed control system is capable of convergence within predefined time, and the predefined-time performance function can ensure that tracking errors fall into a preset range within a specified time ($T_h = 5$ s), thus ensuring transient- and steady-state tracking performance.

Fig. 7 illustrates the approximation effect of the SSNN. F_1 and F_2 are uncertainties in the surge and yaw directions respectively, while $\hat{F}_1$ and $\hat{F}_2$ are approximated outputs of the SSNN. It can be seen that the SSNN has a good capacity of approximation. Fig. 8 illustrates changes in number of SSNN neurons. The initial number of neurons is 41, and the final number of neurons stabilizes at 27 and 26, respectively. Fig. 9 illustrates 2-norm of SSNN weight estimations. From the figure, the 2-norm of SSNN weight estimations converges at about 3 s, and thus the SSNN is effective. Based on Figs. 7−9, the SSNN has a good approximation effect. Number of SSNN neurons can be adjusted online, decreasing by 14 and 15 respectively. This reduces

Table 1　Dynamic model parameters of USV

Parameter	Value	Parameter	Value	Parameter	Value	Parameter	Value
m_0/kg	23.800 0	$X_{\|u\|u}/(\text{kg}\cdot\text{m}^{-1})$	−1.327 4	$N_v/(\text{kg}\cdot\text{m}\cdot\text{s}^{-1})$	0.105 2	$N_{\dot{r}}/(\text{kg}\cdot\text{m}^2)$	−1.000 0
x_g/m	0.046 0	$X_{uuu}/(\text{kg}\cdot\text{s}\cdot\text{m}^{-2})$	−5.866 4	$N_{\|v\|v}/\text{kg}$	5.043 7	$Y_{\|v\|r}/\text{kg}$	−0.845 0
$I_z/(\text{kg}\cdot\text{m}^2)$	1.760 0	$Y_v/(\text{kg}\cdot\text{s}^{-1})$	−0.861 2	$N_{\|r\|v}/(\text{kg}\cdot\text{m})$	0.130 0	$X_u/(\text{kg}\cdot\text{s}^{-1})$	−0.725 5
$X_{\dot{u}}/\text{kg}$	−2.000 0	$Y_{\|v\|v}/(\text{kg}\cdot\text{m}^{-1})$	−36.282 3	$N_r/(\text{kg}\cdot\text{m}^2\cdot s^{-1})$	−1.900 0	$Y_{\|r\|r}/(\text{kg}\cdot\text{m})$	−3.450 0
$Y_{\dot{v}}/\text{kg}$	−10.000 0	$Y_{\|r\|v}/(\text{kg}\cdot\text{m}^{-1})$	−0.805 0	$N_{\|v\|r}/(\text{kg}\cdot\text{m})$	0.080 0		
$Y_{\dot{r}}/(\text{kg}\cdot\text{m})$	0	$Y_r/(\text{kg}\cdot\text{s}\cdot\text{m}^{-1})$	0.107 9	$N_{\|r\|r}/(\text{kg}\cdot\text{m}^2)$	−0.750 0		

Table 2   Control parameters

Parameter	Value	Parameter	Value
σ_{u0}	8.00	$\sigma_{u\infty}$	0.10
σ_{r0}	5.00	$\sigma_{r\infty}$	0.05
k_1	0.50	k_2	1.65
k_u	0.50	k_r	12.00
Υ_1	25.00	Υ_2	25.00
τ_1	0.50	τ_2	0.50
T_h/s	5.00		
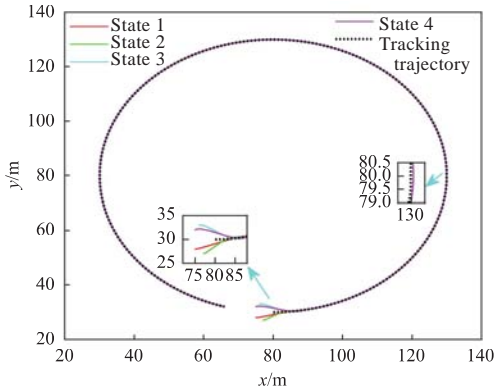
Fig. 4   Trajectory tracking for different initial positions
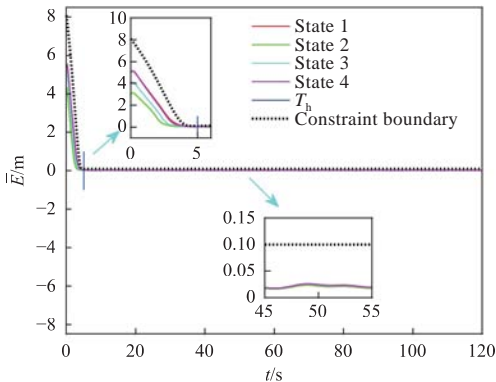
Fig. 5   Tracking error of $\bar{E}$
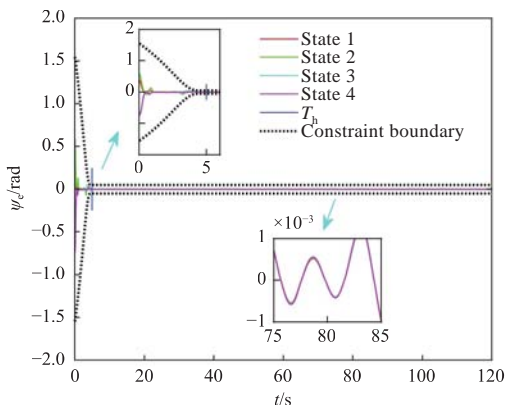
Fig. 6   Tracking error of ψ_e

computational cost of the system effectively.

The initial number of SSNN neurons was set to 41 and the final number of SSNN neurons was 27 and 26, respectively. To demonstrate superiority of the SSNN, we selected RBFNNs with 41 and 27
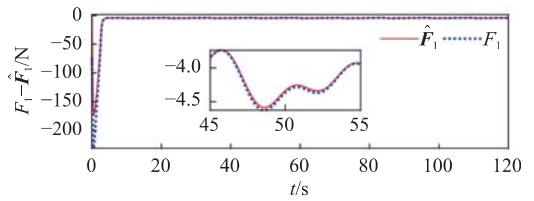
(a) Approximation effect $F_1 - \hat{F}_1$
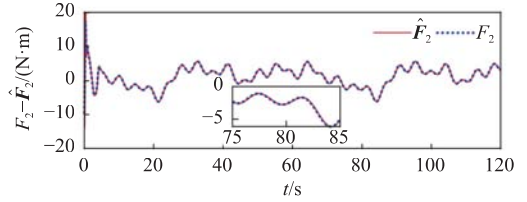
(b) Approximation effect $F_2 - \hat{F}_2$

Fig. 7   Approximation of the self-structuring neural network
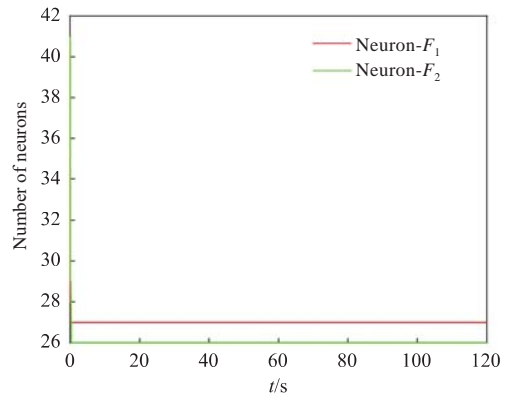
Fig. 8   Number of neurons
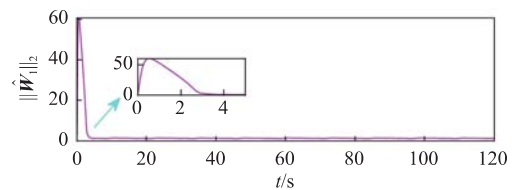
(a) Weight estimation $\|\hat{W}_1\|_2$
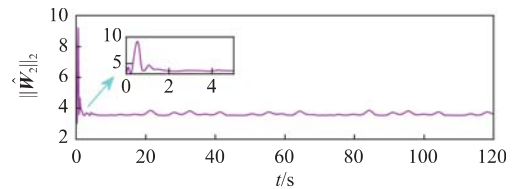
(b) Weight estimation $\|\hat{W}_2\|_2$

Fig. 9   The 2-norm of the SSNNs weight estimation

neurons for comparison. The RBFNNs and the SSNN had the same gains and centers and breadths of Gaussian functions. Fig. 10 illustrates control inputs of different neural networks. The figure shows that control inputs under the SSNN show a stable and smooth curve within 0−6 s, while those under the RBFNNs vary greatly, with sudden changes. Fig. 11 compares the RBFNNs and SSNN in terms of approximation errors. Compared with the RBFNNs containing 41 and 27 neurons, the SSNN yields smaller approximation errors. From

the analysis of approximation effect, SSNN yields a better approximation effect. Moreover, number of SSNN neurons can be adjusted online, which can reduce the computational burden of the closed-loop control system effectively.
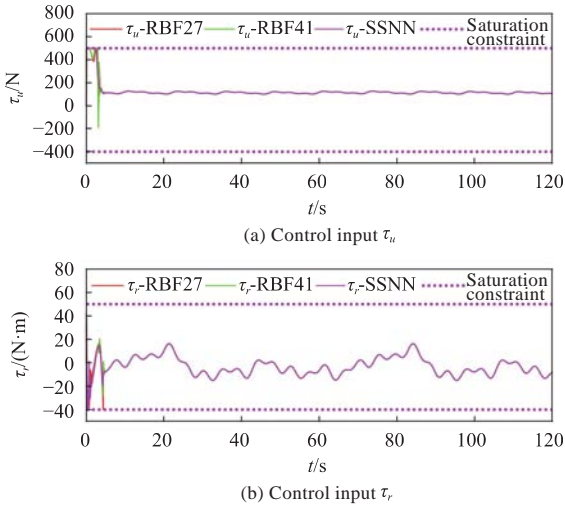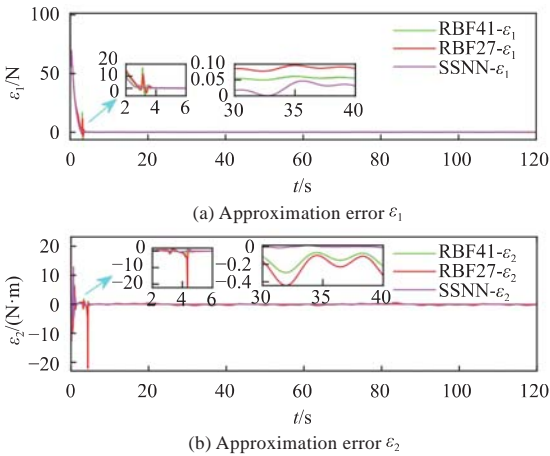

(a) Control input τ_u

(b) Control input τ_r

Fig. 10　Control inputs for different neural networks

(a) Approximation error ε_1

(b) Approximation error ε_2

Fig. 11　Approximate error comparison between RBFNNs and SSNNs

5　Conclusions

This paper proposed a scheme for SSNN-based predefined-time trajectory tracking control. On this basis, it solved such problems of USVs as unknown time-varying disturbances, model uncertainty, and input saturation. As a result, tracking accuracy of the closed-loop control system and convergence rates of system errors are improved. An SSNN was adopted to compensate for unknown dynamics, external time-varying environmental disturbances, and effects of input saturation. Comparison with RBFNNs further verified superiority of the SSNN-based scheme. By using the Lyapunov theory, this paper proved that all signals of the USV trajectory tracking control system were bounded, and that all

system errors converged to a small range within a predefined time. Next, we will study how to reduce communication burden of the control system.

References

[1]　SHAO G M, MA Y, MALEKIAN R, et al. A novel co-operative platform design for coupled USV‐UAV systems[J]. IEEE Transactions on Industrial Informatics, 2019, 15(9): 4913−4922.

[2]　ABDELAAL M, FRÄNZLE M, HAHN A. Nonlinear model predictive control for trajectory tracking and collision avoidance of underactuated vessels with disturbances[J]. Ocean Engineering, 2018, 160: 168−180.

[3]　WANG K, LIU Y H, LI L Y. Vision-based tracking control of underactuated water surface robots without direct position measurement[J]. IEEE Transactions on Control Systems Technology, 2015, 23(6): 2391−2399.

[4]　ZHANG X. Backstepping sliding mode control for trajectory tracking of underactuated USV[J]. Digital Technology and Application, 2020, 38(1): 170−173 (in Chinese).

[5]　PARK B S, YOO S J. An error transformation approach for connectivity-preserving and collision-avoiding formation tracking of networked uncertain underactuated surface vessels[J]. IEEE Transactions on Cybernetics, 2019, 49(8): 2955−2966.

[6]　MU D D, WANG G F, FAN Y S. Trajectory tracking control for underactuated unmanned surface vehicle subject to uncertain dynamics and input saturation[J]. Neural Computing and Applications, 2021, 33(19): 12777−12789.

[7]　ZHU G B, MA Y, LI Z X, et al. Event-triggered adaptive neural fault-tolerant control of underactuated MSVs with input saturation[J]. IEEE Transactions on Intelligent Transportation Systems, 2022, 23(7): 7045−7057.

[8]　YU Y L, SU R B, FENG X, et al. Tracking control of backstepping adaptive path of unmanned surface vessels based on surge-varying LOS[J]. Chinese Journal of Ship Research, 2019, 14(3): 163−171 (in both Chinese and English).

[9]　JIAO J F, HU Z Z. Research on prescribed performance disturbance rejection control of unmanned surface vessels trajectory tracking[J]. Information and Control, 2022, 51(3): 271−279 (in Chinese).

[10]　DAI S L, HE S D, CAI H, et al. Adaptive leader‐follower formation control of underactuated surface vehicles with guaranteed performance[J]. IEEE Transactions on Systems, Man, and Cybernetics: Systems, 2022, 52(3): 1997−2008.

[11]　JIA Z H, HU Z H, ZHANG W D. Adaptive output feedback control with prescribed performance for trajectory tracking of underactuated surface vessels[J]. ISA Transactions, 2019, 95: 18−26.

[12]　HU F F, ZENG C, ZHU G, et al. Trajectory tracking of non-diagonal unmanned underactuated surface vessel

with position and yaw angle constraints[J]. Journal of Terahertz Science and Electronic Information Technology, 2022, 20(4): 332−339 (in Chinese).

[13] DAI S L, HE S D, WANG M, et al. Adaptive neural control of underactuated surface vessels with pre-scribed performance guarantees[J]. IEEE Transactions on Neural Networks and Learning Systems, 2019, 30 (12): 3686 −3698.

[14] LIN J F, LIU H T, TIAN X H. Neural network-based prescribed performance adaptive finite-time formation control of multiple underactuated surface vessels with collision avoidance[J]. Journal of the Franklin Insti-tute, 2022, 359(11): 5174−5205.

[15] QIN H D, LI C P, SUN Y C, et al. Finite-time trajecto-ry tracking control of unmanned surface vessel with er-ror constraints and input saturations[J]. Journal of the Franklin Institute, 2020, 357(16): 11472−11495.

[16] HU M Y, YU S H, LI Y Y, et al. Finite-time trajectory tracking control of full state constrained marine sur-face vessel based on command filter[J]. Journal of Nanjing University of Science and Technology, 2021, 45(3): 271−280 (in Chinese).

[17] ZHANG Z C, WU Y Q. Further results on fixed-time stabilization and tracking control of a marine surface ship subjected to output constraints[J]. IEEE Transac-tions on Systems, Man, and Cybernetics: Systems, 2021, 51(9): 5300−5310.

[18] HE S D, DONG C, DAI S L. Adaptive neural forma-tion control for underactuated unmanned surface vehi-cles with collision and connectivity constraints[J]. Ocean Engineering, 2021, 226: 108834.

[19] GHOMMAM J, SAAD M, MNIF F. Prescribed perfor-mances based fuzzy-adaptive output feedback contain-ment control for multiple underactuated surface vessels [J]. Ocean Engineering, 2022, 249: 110898.

[20] LIU H T, LI Y Z, TIAN X H. Practical finite-time event-triggered trajectory tracking control for underac-tuated surface vessels with error constraints[J]. IEEE Access, 2022, 10: 43787−43798.

[21] ZHANG Q, ZHU Y P, MENG X F, et al. Finite time trajectory tracking of underactuated ship based on adaptive neural network[J]. Chinese Journal of Ship Research, 2022, 17(4): 24−31 (in both Chinese and English).

[22] ZHANG K, WANG Y L, LIU Z Q. Trajectory tracking control of underactuated unmanned surface vehicles with disturbance observer[J]. Ship Science and Tech-nology, 2019, 41(12): 127−132, 139 (in Chinese).

[23] GUO G, ZHANG P F. Asymptotic stabilization of US-Vs with actuator dead-zones and yaw constraints based on fixed-time disturbance observer[J]. IEEE Transac-tions on Vehicular Technology, 2020, 69(1): 302−316.

[24] XIE W, REIS J, CABECINHAS D, et al. Design and experimental validation of a nonlinear controller for underactuated surface vessels[J]. Nonlinear Dynamics, 2020, 102(4): 2563−2581.

[25] ZHANG G Q, LIU S, ZHANG X K. Adaptive distrib-uted fault-tolerant control for underactuated surface ve-

[26] ZHANG C J, WANG C, WANG J Q, et al. Robust adaptive position tracking control of underactuated un-manned surface vehicle[J]. Acta Armamentarii, 2020, 41(7): 1393−1400 (in Chinese).

[27] WANG N, JOO ER M. Self-constructing adaptive ro-bust fuzzy neural tracking control of surface vehicles with uncertainties and unknown disturbances[J]. IEEE Transactions on Control Systems Technology, 2015, 23 (3): 991−1002.

[28] ZHANG G Q, CHU S J, JIN X, et al. Composite neu-ral learning fault-tolerant control for underactuated ve-hicles with event-triggered input[J]. IEEE Transactions on Cybernetics, 2021, 51(5): 2327−2338.

[29] XIE S Z, CHEN Q. Adaptive nonsingular predefined time control for attitude stabilization of rigid space-crafts[J]. IEEE Transactions on Circuits and Systems II: Express Briefs, 2022, 69(1): 189−193.

[30] YANG H J, YE D. Adaptive fixed-time bipartite track-ing consensus control for unknown nonlinear multi-agent systems: an information classification mecha-nism[J]. Information Sciences, 2018, 459: 238−254.

[31] ZHANG L Y, LIU H, TANG D F, et al. Adaptive fixed-time fault-tolerant tracking control and its application for robot manipulators[J]. IEEE Transactions on Indus-trial Electronics, 2022, 69(3): 2956−2966.

[32] POLYCARPOU M M, IOANNOU P A. A robust adap-tive nonlinear control design[J]. Automatica, 1996, 32 (3): 423−427.

[33] ZHANG C J, WANG C, WEI Y J, et al. Robust trajec-tory tracking control for underactuated autonomous surface vessels with uncertainty dynamics and unavail-able velocities[J]. Ocean Engineering, 2020, 218: 108099.

[34] CHEN L P, CUI R X, YANG C G, et al. Adaptive neu-ral network control of underactuated surface vessels with guaranteed transient performance: theory and ex-perimental results[J]. IEEE Transactions on Industrial Electronics, 2020, 67(5): 4024−4035.

[35] SKJETNE R, FOSSEN T I, KOKOTOVIĆP V. Adap-tive maneuvering, with experiments, for a model ship in a marine control laboratory[J]. Automatica, 2005, 41 (2): 289−298.

[36] ZHENG Z W, JIN C, ZHU M, et al. Trajectory track-ing control for a marine surface vessel with asymmet-ric saturation actuators[J]. Robotics and Autonomous Systems, 2017, 97: 83−91.

[37] HUA C C, MENG R, LI K, et al. Dynamic event-based adaptive finite-time tracking control for nonlin-ear stochastic systems under state constraints[J]. IEEE Transactions on Systems, Man, and Cybernetics: Sys-tems, 2022, 52(11): 7201−7210.

[38] ZHANG L L, CHE W W, CHEN B, et al. Adaptive fuzzy output-feedback consensus tracking control of nonlinear multiagent systems in prescribed perfor-mance[J]. IEEE Transactions on Cybernetics, 2023, 53 (3): 1932−1943.

基于输入饱和的欠驱动水面舰艇
预定义时间跟踪控制

黄秀颖[1]，刘海涛[*1,2]，田雪虹[1,2]

1 广东海洋大学 机械工程学院，广东 湛江 524088
2 广东海洋大学深圳研究院，广东 深圳 518120

摘　要：［**目的**］为解决欠驱动水面舰艇（USV）在模型不确定性、强耦合特性和控制器输入饱和情况下的轨迹跟踪问题，提出基于输入饱和的 USV 预定义时间跟踪控制方法。［**方法**］针对 USV 模型具有非零对角项和强耦合特性问题，引入坐标变换，将系统模型转变为斜对角形式；将预定义时间性能函数与障碍 Lyapunov 函数（BLF）结合，保证瞬态和稳态的跟踪性能；利用自组织神经网络（SSNN）降低未知外部环境扰动和复杂的连续未知非线性项以及输入饱和产生的影响，以保证控制系统的跟踪精度，并且在线调整优化 SSNN 的神经元数目，减少控制系统的计算负担。［**结果**］基于 Lyapunov 稳定性理论，证明了闭环系统在预定义时间内是有界稳定的，跟踪误差始终保持在约束范围内。［**结论**］仿真结果表明，所提控制策略是有效的，其具有良好的跟踪性能。

关键词：欠驱动水面舰艇；预定义时间性能函数；障碍 Lyapunov 函数；自组织神经网络；输入饱和；预定义时间控制